Excess melanin precursors rescue defective cuticular traits in *stony* mutant silkworms probably by upregulating four genes encoding RR1-type larval cuticular proteins

Liang Qiao [b+,*], Zheng-wen Yan [a+], Gao Xiong [a], You-jin Hao [a], Ri-xin Wang [a], Hai Hu [a], Jiang-bo Song [a], Xiao-ling Tong [a], Lin-rong Che [b], Song-zhen He [a], Bin Chen [b], James Mallet [c], and Cheng Lu [a], Fang-yin Dai [a,*]

[a] State Key Laboratory of Silkworm Genome Biology; Key Laboratory of Sericultural Biology and Genetic Breeding, Ministry of Agriculture; College of Biotechnology, Southwest University, Chongqing 400716, China.

[b] Chongqing Key Laboratory of Vector Insects, Institute of Entomology and Molecular Biology, College of Life Sciences, Chongqing Normal University, Chongqing, 401331, China.

[c] Department of Organismic and Evolutionary Biology, Harvard University, Cambridge, MA 02138, USA.

Running title: Excess melanin rescues cuticular defects in silkworms

[+] Equally contributed

[*] Corresponding Authors.

E-mail address: qiaoliangswu@163.com, fydai@swu.edu.cn

Abstract

Melanin and cuticular proteins are vital cuticle components in insects. Cuticular defects caused by mutations in cuticular protein-encoding genes can obstruct melanin deposition. The effects of changes in melanin on the expression of cuticular protein-encoding genes, the cuticular and morphological traits, and the origins of these effects are unknown. We found that the cuticular physical characteristics and the expression patterns of larval cuticular protein-encoding genes markedly differed between the melanic and non-melanic integument regions. By using four *p* multiple-allele color pattern mutants with increasing degrees of melanism ($+^{p}$, p^{M}, p^{S}, and p^{B}), we found that the degree of melanism and the expression of four RR1-type larval cuticular protein-encoding genes (*BmCPR2*, *BmLcp18*, *BmLcp22*, and *BmLcp30*) were positively correlated. By modulating the content of melanin precursors and the expression of cuticular protein-encoding genes in cells in tissues and *in vivo*, we showed that this positive correlation was due to the induction of melanin precursors. More importantly, the melanism trait introduced into the *BmCPR2* deletion strain Dazao-*stony* induced up-regulation of three other similar chitin-binding characteristic larval cuticular protein-encoding genes, thus rescuing the cuticular, morphological and adaptability defects of the Dazao-*stony* strain. This rescue ability increased with increasing melanism levels. This is the first study reporting the induction of cuticular protein-encoding genes by melanin and the biological importance of this induction in affecting the physiological characteristics of the cuticle.

Keywords: Melanic coloring; Cuticle features; Cuticular protein-encoding genes; Induction;

Bombyx mori

1. Introduction

Melanic color patterns play important roles in many adaptive processes in insects, such as mimicry, mating preference, and the ability to resist pathogens and UV thermoregulation (Hu et al., 2013; Liu et al., 2015a; Mallet and Hoekstra, 2016; True, 2003; Wilson et al., 2001; Wittkopp et al., 2003).

The roles of melanism in insects rely on not only the integrity of melanin biosynthesis and regulatory pathways (Futahashi and Fujiwara, 2005; Wittkopp and Beldade, 2009; Wittkopp et al., 2003) but also the presence of the 'platform' on which melanin relies (Andersen, 2010; Moussian, 2010; Van Belleghem et al., 2017; Wittkopp and Beldade, 2009; Wittkopp et al., 2003). In insects, the cuticle is the most important platform for the formation of the melanic color pattern (Andersen, 2010; Hopkins and Kramer, 1992; Moussian, 2010). During the shaping of the cuticle, the maintenance of the cuticle's features depends on cuticular proteins and their interactions with other components (Andersen, 2010; Chaudhari et al., 2011; Guan et al., 2006; Hopkins and Kramer, 1992; Moussian, 2010; Noh et al., 2016; Suderman et al., 2006).

Because of the critical roles of cuticular proteins in cuticle development, if the genes including these proteins lose their functions, the defective cuticle affects the deposition and attachment of melanin, thereby influencing the formation of the melanic color pattern (Arakane et al., 2012; Kanekatsu et al., 1988; Noh et al., 2015; Oota and Kanekatsu, 1993; Xiong et al., 2017). Little is known about how cuticular protein-encoding genes respond to

alterations in melanin biosynthesis or regulatory pathways.

Recently, several reports have shown that the abundance of cuticular protein-encoding genes in different colored integuments varies in insect species, and that these genes are up-regulated in the melanic cuticle regions (Futahashi et al., 2012; He et al., 2016; Jan et al., 2017; Wu et al., 2016). Some of those cuticular protein-encoding genes have similar expression patterns and functions (Liang et al., 2010; Nakato et al., 1994; Nakato et al., 1997; Okamoto et al., 2008; Qiao et al., 2014; Shofuda et al., 1999; Tang et al., 2010). These studies suggest a likely relationship between the promotion of melanism and the expression of cuticular protein-encoding genes. Prior to this study, the potential relationships among cuticular protein-encoding genes were unclear. Additionally, when melanism signaling and defects in cuticle proteins occur simultaneously, the net effects on the morphological and physiological traits are also unclear.

In the Lepidoptera model *Bombyx mori*, an intriguing phenomenon has been reported in which the larval melanic mutant *Striped* (p^S, 2-0.0) reverses the malformed body shape and the adaptability defects of the *stony* mutant (*st*, 8-0.0) (Dai et al., 2000; Xiang, 1995). A recent study has reported that the transcription factor *Apontic-like*, which increases the expression of melanin synthesis genes in epidermal cells, is responsible for the p^S mutant phenotype (Yoda et al., 2014). Multiple alleles exist with different degrees of melanism at the *p* locus, including p^B and p^M (Banno et al., 2005; Xiang, 1995; Yoda et al., 2014). The *stony* mutant (*st*, 8-0.0) is caused by a deletion of a portion of a RR1-type larval cuticular protein-encoding gene *BmCPR2* (*BmLcp17*). The *stony* mutant has is hard and tight to the touch, and has imbalanced ratios of the lengths of the internodes (I) and the intersegment folds (IF) (I/IF of

approximately 1.6 in the *stony* mutation and approximately 4 in the wild-type strain), bulges at the intersegment folds, and severely altered locomotion and behavioral activities in the larval stage (Qiao et al., 2014). The similarities in the gene expression patterns (Fig. S1) and functional characteristics of the other RR1-type larval cuticular protein-encoding genes (*Lcps*), *BmLcp18*, *BmLcp22*, and *BmLcp30* also suggest that they may play very similar roles to those of *BmorCPR2* in shaping the larvae cuticle (Dong et al., 2016; Liang et al., 2010; Nakato et al., 1994; Nakato et al., 1997; Okamoto et al., 2008; Qiao et al., 2014; Shofuda et al., 1999; Tang et al., 2010). These findings can be linked through the epistasis of p^S to *stony* (Dai et al., 2000), and provide highly useful genetic resources for exploring the interactions between melanin and cuticular protein-encoding genes.

In the present study, we found that the transcript levels of *BmorCPR2*, *BmLcp18*, *BmLcp22*, and *BmLcp30* were positively correlated with the degree of melanism of the larval cuticle. This positive correlation was due to the simultaneous induction of these genes by melanin precursors. Moreover, after melanism induction in the *stony* mutant, the cuticle deficiency was rescued through functionally similar compensation by up-regulated *BmLcp18*, *BmLcp22*, and *BmLcp30*. These findings provide new evidence indicating that melanism is a beneficial trait and also deepen understanding of the interactions among the genetic factors shaping morphological features in Lepidopterans.

2. Materials and Methods

2.1. Silkworm strains

The wild-type strain Dazao ($+^p$) and melanic mutant strains p^M, p^S, and p^B (Banno et al.,

2005; Xiang, 1995; Yoda et al., 2014) were used in this study. The pigment intensity was measured as the mean OD value in Image J (https://imagej.nih.gov/ij/). In terms of the degree of melanism, the body color of an individual homozygous at the p^M or p^S loci is darker than that of a heterozygous individual (Banno et al., 2005; Xiang, 1995). The albinism mutant *albino* (*al*) (Banno et al., 2005; Fujii et al., 2013), the non-diapause wild-type strain N4 (used for melanin inhibition treatment), the *BmCPR2* deletion strain, and the Dazao-*stony* strain (a near isogeneic line of Dazao, which has been backcrossed with Dazao for more than 26 generations) were supplied by the Silkworm Gene Bank at Southwest University. The N4 strain and *al* mutant were fed an artificial diet at 28 □. All other strains were fed fresh mulberry leaves under a 12 h/12 h light/dark photoperiod at 24 °C.

2.2. Chemicals and cell lines

L-Dopa, dopamine, tetrahydrofolic acid (BH_4, a cofactor for the synthesis of melanin), and 2,4-diamino-6-hydroxypyrimidine (DAHP, an inhibitor of guanylate cyclase hydrolase (GTPCHI), an important rate-limiting enzyme in the synthesis of BH_4 (Delgado-Esteban et al., 2002; Mitchell et al., 2003) in melanin metabolism) were purchased from Sigma-Aldrich (St. Louis, MO, USA). The *Bombyx mori* embryonic (*BmE*) cell line was established in our laboratory more than 10 years ago and was used for the basal expression analysis of *BmCPR2*, *BmLcp18*, *BmLcp22*, *BmLcp30*, and *BmCPH24* (Fig. S2).

2.3. Chitin content determination

Melanic and non-melanic larval cuticles were dissected, and the attached tissues were also removed; samples were then washed with double distilled H_2O and dried at 60 □. Dried cuticles were weighted with an analytical balance (METTLER-MS105DU, Germany). The

extraction and determination of chitin content were conducted as described by Kunyan Zhu *et al* (Zhang and Zhu, 2006) with slight modifications. Three or four biological replicates for each sample were examined.

2.4. Scanning electron microscopic analysis

Melanic and non-melanic larval cuticles were dissected, and the attached tissues were also removed; samples were then washed with double distilled H_2O and gradually dehydrated according to Hu's method (Hu et al., 2009). Samples were sputter-coated with gold with a Hitachi E-1010 high-resolution sputter coater (Hitachi, Japan) and observed under a Hitachi S-3000N scanning electron microscope (Hitachi, Tokyo, Japan).

2.5. Mating combinations and progeny phenotype identification

The p^S and p^M strains were crossed with the Dazao-*stony* strain to generate the F_1 generation. The F_2 generation was produced by F_1 self-crossing F_1. Individuals at day 5 of the 5^{th} instar (the larval stage is approximately 8 days in the experimental conditions of our laboratory) of F_2 were collected for further use. The p^B strain was crossed with the Dazao-*stony* strain to generate F_1 progeny, which were then mated with the Dazao-*stony* strain to generate the BC_1 generation. The BC_1 generation was fed until day 5 of the 5^{th} instar.

Individuals of the F_2 or BC_1 generations were separated according to cuticle pigmentation. Subsequently, phenotypes were classified by morphological characteristics, and I/IF ratios in the second, third, and fourth abdominal segments, according to a previously described method (Qiao et al., 2014).

2.6. Genotyping

Because the p^S, p^M, and p^B mutations are alleles at the *p* locus, they should be located in

proximity on chromosome 2 (Banno et al., 2005; Xiang, 1995; Yoda et al., 2014). According to the gene sequence of the p^S allele, 11 PCR primer pairs in a 12.4 kb genomic region (from 3.9 kb upstream of the translation initiation site (ATG) of *apt-like* to 8.5 kb downstream of the initial codon) were used. PCR screening was performed for p^M, p^S, p^B, and the Dazao-*stony* strain to obtain molecular markers of polymorphism for the *p* locus. We found a molecular marker at 1.47 kb (within the intron region) downstream of the initial codon. Similarly, a PCR-based molecular marker was also designed within genomic region of *BmCPR2* to screen for polymorphism at the *stony* locus, and the primers were used to analyze CDS sequence differences between *stony* and wild-type as in our previous study (Qiao et al., 2014). The primers used in this study are listed in Table S1.

2.7. Analysis of phenotype, genotype, and gene expression

Day 5 5th instar larvae of the Dazao and Dazao-*stony* strains (the larval stage is approximately 8 days in the experimental conditions of our laboratory) were selected for cuticle dissection. The cuticles of the semi-lunar marking region and the non-melanic portion between the paired semi-lunar markings were dissected. Gene expression levels of *BmCPR2* (KF672849.1), *BmLcp18* (NW_004582021.1), *BmLcp22* (NW_004582025.1), *BmLcp30* (NW_004582025.1), *BmCPR68* (NM_001173219), *BmCPR3* (NM_001173273), *BmCPR129* (NM_001173170), *BmCPG13* (NM_001173319), *BmCPH25* (NM_001173281), *Bmyellow* (DQ358085.2), *BmDDC* (NW_004582031.1), and *Bmlaccase 2* (NW_004582017.1) in these regions were compared. Gene expression patterns were determined for the dorsal epidermis of abdominal segments (from semi-lunar marking to star marking) from day 5 5th instar larvae of Dazao, p^S/+, p^M/+, and p^B/+ strains. The 2nd instar larvae at day 1 were also analyzed in the *al*

and Dazao strains. The dorsal epidermis regions (from the semi-lunar marking to the star marking) were collected from the BC_1 and F_2-generation of the $p^B/+^{pB}$, $+^{st}/st$, $p^B/+^{pB}$, *st/st*, p^S/p^S, *st/st*, $p^S/+^{pS}$, *st/st*, p^M/p^M, *st/st* and $p^M/+^{pM}$, and *st/st* genotypes for gene expression analysis. For all genotyped individuals, the I/IF ratios were also analyzed in Image J (https://imagej.en.softonic.com/).

2.8. Confocal microscopy analysis

The cuticles of day 5 5th instar larvae (strains: p^S, Dazao, Dazao-*stony*, and $p^B/+^{pB}$,+*st/st*, $p^B/+p^B$, *st/st*, p^S/p^S, *st/st*, $p^S/+^{pS}$, *st/st*, p^M/p^M, *st/st*, $p^M/+^{pM}$, *st/st*, $+^p/+^p$, and *st/st* in BC_1 and cross F_2 progeny) were dissected. After removal of attached tissues, such as the dermis and muscles, the cuticle was washed for 5 min in 1× PBS buffer and fixed in 4% paraformaldehyde for 1 h at 4 □. After being washed three times in 1× PBS (5 min each time), the cuticles were air-dried and embedded in embedding agent (SAKURA Tissue-Tek O.C.T compound, USA) for 30 minutes at -20 □. Then 4 μm slices were prepared on a HM525 NX freezing microtome (Thermo Scientific, USA). Confocal imaging was performed with a FV3000 (OLYMPUS, Japan) confocal microscope (objective lens: 60×, zoom: 1.67×) and then merged in Z-Dimension mode. The cuticle thickness was measured with Image J (https://imagej.en.softonic.com/). Three biological replicates were examined for each sample, and more than three observations were made for repeat samples.

2.9. Melanin precursor promoting and inhibiting treatments

L-Dopa and dopamine solutions were prepared according to Futahashi, with slight modifications (Futahashi and Fujiwara, 2005). L-Dopa and dopamine solutions were filtered with 0.22 μm membranes before use. *BmE* cells were washed three times with Grace medium

199 without melanin precursors to remove metabolites and other contaminants on the cell surfaces.
200 Medium (0.8 mL) containing L-Dopa or dopamine was added separately into each well of a
201 24-well plate. Medium without melanin precursors was used as a control for gene expression
202 analysis. Culture plates were sealed with tape, wrapped with foil, and incubated at 28 □ for
203 24 h for gene expression analysis. For BH_4 feeding assays, a 30 mM working solution was
204 prepared by dissolving tetrahydrofolic acid into double distilled H_2O and spreading it on an
205 artificial diet for the *al* mutant strain. As a control, the *al* mutant strain (with albinism and a
206 porous cuticle, owing to a mutation in the sepiapterin reductase gene, which leads to
207 insufficient synthesis of the cofactor BH_4 during the synthesis of melanin precursors (Banno
208 et al., 2005; Fujii et al., 2013)), fed with an artificial diet treated only with double distilled
209 H_2O, was used. Phenotypes were recorded from the 2^{nd} instar stage, and expression of
210 cuticular protein-encoding genes was analyzed.

211 To perform the melanism-inhibition experiments, we used the wild-type strain N4 (melanic
212 body color at 2^{nd} instar stage). Newly hatched larvae were divided into treatment and control
213 groups. Individuals in the treatment group were fed an artificial diet containing DAHP
214 (dissolved in 0.1 M NaOH), and individuals in the control group were fed an artificial diet
215 containing 0.1 M NaOH.

216 To prepare artificial diets with or without DAHP, the following procedures were performed:
217 for the treatment group, 2.5 g DAHP was dissolved in 0.1 M NaOH (with a total volume of
218 150 mL); then 50 g artificial food was added and mixed in, and the diet was further treated at
219 98 □ for 25 min. For the control group, although no DAHP was added, the other treatment
220 procedures were the same. The larvae were separately fed artificial feed once daily for three

consecutive days. The day 1 2nd instar larvae were selected for phenotype and expression analysis.

2.10. Integument culture

The procedures for integument cultures were carried out according to Futahashi and Fujiwara (Futahashi and Fujiwara, 2006) with minor modifications. The Dazao strain at day 5 5th instar was selected to dissect the non-melanic integuments on the dorsal side of the 3rd–4th abdominal segments. After removal of the muscle, trachea, and fat body, the tissues were cut into rectangles (4 mm × 4 mm), washed five times in 1× PBS, and dried on sterile filter paper. Three to six pieces of integuments were placed in 1.5 ml microcentrifuge tubes, and 600 μl Grace medium (GIBCO BRL) was added, including 6 μg/ml phenylthiourea (to prevent phenol oxidase activity), penicillin-streptomycin (100 U/ml), streptomycin (0.1 mg/ml), and 5 mM L-Dopa or dopamine. The mixture was gently stirred to disperse the integuments, sealed to avoid light, and then placed on a shaker and incubated at 24 ℃ for 24 h at a speed of 80 rpm/min (with the angle not exceeding 30 degrees during incubation). Grace medium without L-Dopa and dopamine was used as the control. After incubation, the dermal cell layers on the integuments were gently scraped off and washed with 1× PBS. The degree of melanism in the cuticle was determined under a stereomicroscope (OLYMPUS, Japan). Gene expression patterns were detected by quantitative reverse transcription-PCR (qRT-PCR). Phenotypic observations and gene expression detection in the treatment group and control group were performed on at least three biological replicates.

2.11. Overexpression of BmCPH24

Overexpression vectors for *BmCHP24* (larval cuticular protein-encoding genes) and

243 *piggyBac* (*A3*-EGFP, *IE1-BmCPH24-SV40*) were constructed in our laboratory by Xiong *et al*
244 (Xiong et al., 2017). The empty vector without *BmCPH24* was used as a control. One
245 microgram of overexpression vector and control vector were transfected into *BmE* cells with
246 X-tremeGENE HP (Roche, Basel, Switzerland). Two days post-transfection, transfected cells
247 were observed, and cells with high fluorescence intensity were collected for RNA extraction.
248 The expression of cuticular protein genes in overexpression cells and controls was determined
249 with qRT-PCR. Primers are listed in Table S1.

250 *2.12. Quantitative RT–PCR*

251 Total RNA extraction, reverse transcription, and qRT-PCR were performed as described
252 previously (Qiao et al., 2014). Three biological replicates were prepared for each condition,
253 and the house-keeping gene *BmRPL3* was used as the internal control. Primers used are listed
254 in Table S1.

255

256 **3. Results**

257 *3.1. Cuticle physical characteristics are entirely distinct between melanic and non-melanic*
258 *cuticular regions*

259 The cuticle section slices showed that the melanin protrusions were deposited in the
260 epicuticle of the p^S strain and the lunar marking of the Dazao strain (Figure 1A). The
261 thickness of the melanic cuticle was also greater than that of the non-melanic cuticle (Figure
262 1B). Moreover, the surface nanostructures were much denser in the melanic regions than in
263 the non-melanic regions, regardless of strain (Fig. S3A), owing to the deposition of melanin
264 in the epicuticle. The content of chitin (a major component for cuticle construction, which is

closely related to cuticle pigmentation (Moussian et al., 2005; Moussian et al., 2006)) was correspondingly increased in the melanic cuticle (Fig. S3B). In non-melanic regions of the *stony* mutant, the arrangement of the procuticle was disordered, and damage to the exocuticle was observed (Figure 1A). The intersegments cuticle of the stony mutant was the thinnest relative to that in the intersegments cuticles of p^S, Dazao, and the semi-lunar marking cuticular region of Dazao and Dazao-*stony* (Figure 1B). However, the disordered arrangement of the procuticle in the melanic semi-lunar marking region of the *stony* mutant was not observed (Figure 1A). The cuticle was also thicker than that in the non-melanic region of the Dazao-*stony* strain (Figure 1B).

3.2. Correlation of larval cuticular protein-encoding gene expression with cuticle melanism

The expression levels of *BmCPR2*, *BmLcp18*, *BmLcp22*, and *BmLcp30* were higher in the melanic regions than the non-melanic regions (Figure 2). We further investigated the expression patterns of those genes by using four alleles of the *p* locus (Dazao ($+^p$), p^M, p^S, and p^B) with greater melanin accumulation than that in the Dazao strain (Figure 3A). Expression levels of *BmorCPR2*, *BmLcp18*, *BmLcp22*, and *BmLcp30* were gradually and up-regulated with increasing melanism in the cuticle (Figure 3B, Fig. S4). These results showed that the expression of *BmorCPR2*, *BmLcp18*, *BmLcp22*, and *BmLcp30* correlated positively with the degree of melanism (Figure 3, Fig. S4).

3.3. Effects of melanin precursors on the expression of cuticular protein-encoding genes

The basal expression of four larval cuticular protein-encoding genes was analyzed in *BmE* cells (Fig. S2), thus indicating that regulatory pathways controlling the expression of these cuticular protein-coding genes were present in this cell line. After incubation of *BmE* cells

with melanin precursors, the expression of cuticular protein-encoding genes was higher in cells treated with either L-Dopa or dopamine than in the control cells (Figure 4A). In addition, when the 2nd instar *al* mutant was treated with BH_4, the larvae had a normal melanic body color (Fujii et al., 2013), and the expression of four RR1-type *BmLcps* was higher than in the control group (Figure 4B). Moreover, in the wild-type 2nd instar larvae treated with DAHP, the cuticles lost their original melanic body color (Tong et al., 2018), and the expression of four RR1-type *Bm Lcps* was lower than that in the control group (Figure 4C). Furthermore, regarding the unchanged melanin precursor content, the expression of *BmLcp18*, *BmLcp22*, and *BmLcp30* was not affected by the deletion of *BmLcp17* (Fig. S5). The larval cuticular protein-encoding gene *BmCPH24* (with a similar expression pattern to those of the four RR1-type *BmLcps*. Loss of function of *BmCPH24* also produced a *stony*-like phenotype, but with more pronounced defects (Xiong et al., 2017)) was overexpressed, yet had no effect on the expression of the four RR1-type *BmLcp* genes (Fig. S6).

3.4. Phenotypic observation and expression of cuticular protein-encoding genes after L-Dopa and dopamine treatment

After incubation with 5 mM melanin precursors for 24 h, the cuticles of larvae showed melanism, whereas the control group did not (Figure 5A). Simultaneously, the expression of *BmCPR2*, *BmLcp18*, *BmLcp22*, and *BmLcp30* in the melanin precursor treatment groups was higher than that in the control group (Figure. 5B).

3.5. Complete masking of stony phenotypes by the p^B locus

We assessed the effects of modulating the melanic background on the phenotypic defects caused by the deletion of *BmorCPR2*. After mating of the p^B and *stony* parental strains (553

309 BC_1 individuals), the percentage of BC_1 individuals with melanism and a normal body shape
310 in the backcrossed population was 52% (ratio 290:553 = 2.098:4; χ^2 = 304.8, df = 1, $p < 0.01$)
311 but theoretically should have been 25% (ratio 1:4) (Table 1). No individuals with the melanic
312 cuticle and *stony*-type body shape were found (ratio 0:553, χ^2 = 304.8, df = 1, $p < 0.01$), but
313 theoretically these individuals should have been present at 25% (ratio 1:4), equivalent to the
314 number of individuals with melanic cuticle and normal body shape (Table 1). Genotyping
315 results showed that approximately 25.68% (ratio 142:553 = 1.027:4) of the individuals
316 showing a melanic color and normal body shape in the BC_1 population from the p^B×*stony*
317 cross had the $p^B/+^{pB}$, *st/st* genotypes (Figure 6A, Table 4). The I/IF ratio was 4, which was
318 similar to that in $p^B/+^{pB}$, $+^{st}/st$ individuals (26.94%, ratio 149:553 = 1.070:4) and was also not
319 significantly different from that in the wild-type individuals (Figure 6B) (Qiao et al., 2014).
320 Together, these results suggested that defective phenotypes were masked when the p^B locus
321 was induced into the *stony* mutant.

322 *3.6 No typical stony-type phenotype was observed in st/st genotyped progeny containing p^S or*
323 *p^M loci*

324 In the cross of p^S×*stony* (331 F_2 individuals), 64.3% of F_2 progeny showed a p^S-type color
325 pattern and normal body shape (ratio 213:331 = 10.296:16; theoretical ratio, 9:16) (Table 2).
326 We did not find individuals with a typical *stony*-type body shape and defective adaptability
327 under the melanism background (theoretical ratio, 3:16) (χ^2 = 65.9, df = 1, $p < 0.01$, see Table
328 2). Genotyping analysis indicated that 57.7% (ratio 191:331 = 9.233:16) of individuals with
329 the $p^S/\_$, $+^{st}/\_$ genotype (Table 4, Fig. S7A), 6.04% (ratio 20:331 = 0.967:16) of individuals
330 with the p^S/p^S, *st*/*st* genotype (Figure 6A, Table 4), and only 0.604% (ratio 2:331 = 0.097:16)

of individuals with the $p^{S}/+^{pS}$, *st/st* genotype had melanic color and a normal body shape (Table 4). In individuals genotyped as p^{S}/p^{S}, *st/st*, the I/IF ratio was 3.3 (Figure 6B). The I/IF ratio was lower than that of $p^{S}/\_$, $+^{st}/\_$ individuals (Figure 6B) but higher than that reported for the *stony* mutant (1.6) (Qiao et al., 2014). Despite the slightly smaller body size of the p^{S}/p^{S},*st/st* individuals, their body shape was essentially normal (Figure 6A). However, we found that 10.88% of F_2 progeny (ratio = 1.740:16) had a lighter melanic color and smaller body size (Figure 6A, Table 2). Their intersegment folds were slightly bulged, and the intersegment fold length was much shorter than that of the internodes (Figure 6). Correspondingly, their phenotypes slightly resembled the morphological features of the *stony* mutant (Figure 6, Table 2). The genotype of these individuals was $p^{S}/+^{pS}$, *st*/*st*, and their I/IF ratio was approximately 2.7 (Figures 6, Table 4), a value much higher than that of the *stony* mutant.

In the p^{M}×*stony* cross (437 F_2 individuals), 62.9% of F_2 progeny exhibited a p^{M}-type color pattern, and normal body shape or some other subtle *stony* features (very slight bulges) (ratio 275:437 = 10.068:16, the theoretical ratio is 9:16) (Table 3). In these progeny, the number of $p^{M}/\_$, and $+^{st}/_$genotyped individuals was 244 (55.8% ≈ 9:16, Table 4, Fig. S7B), and the I/IF ratio was approximately 3.9 (Figure 6B). The genotypes for individuals with subtle *stony* features (very slight bulges) were mainly p^{M}/p^{M}, *st/st* (6.63%, ratio 29:437 = 1.062:16), with a small amount of $p^{M}/+^{pM}$, *st/st* (0.458%, ratio 2:437 = 0.073:16). The I/IF ratio of p^{M}/p^{M}, *st/st* progeny was approximately 2.8, in agreement with their phenotypes (Figure 6A and 6B). In addition, 11.7% (ratio 51:437 = 1.86:16) of individuals in the F_2 population were much lighter but exhibited unusual morphological features (Table 3). Their intersegment folds were more

bulged and had longer length proportions. Their genotypes were identified as $p^M/+^{pM}$, *st/st*, and the I/IF ratio was 1.8 (Figures 6A and 6B, Table 4), a value close to that of the *stony* mutant. Their body features resembled the phenotype of the *stony* mutant (Table 3). However, individuals with the p^M-type color pattern with the typical *stony* morphologic features and defective adaptability were not present among progeny from the $p^M \times$ *stony* cross (theoretical ratio, 3:16) ($\chi^2 = 85.4$, df = 1, $p < 0.01$, see Table 3).

3.7 Cuticle slices and gene expression analysis of melanic progeny from BC_1 and F_2 crosses involving stony and p locus alleles

In BC_1 and F_2 progeny of the genotype *st/st* with melanic cuticle, we found that the epicuticle of $p^B/+^{pB}$, $+^{st}/st$, and $p^B/+^{pB}$, *st/st* individuals densely covered the melanin protrusions. The structures of their procuticles were well organized. In contrast, the procuticle structures of $+^p+^p$, *st/st* individuals were not well organized, and some damage was observed in the exocuticle. In addition, the cuticle thickness of the $p^B/+^{pB}$, $+^{st}/st$, and $p^B/+^{pB}$, *st/st* individuals was greater than that of the $+^p+^p$, *st/st* individuals (Figure 7A-7B). Although the melanin protrusions were less in p^S/p^S, *st/st* individuals than $p^B/+^{pB}$, $+^{st}/st$ and $p^B/+^{pB}$, *st/st* individuals, no disordered procuticles were observed (Figure 7A). The cuticle thickness was slightly less than that of the $p^B/+^{pB}$, $+^{st}/st$ and $p^B/+^{pB}$, *st/st* individuals. The cuticular melanin protrusions in the $p^S/+^{pS}$, *st/st* individuals were less than those in the p^S/p^S, *st/st* individuals, and the procuticles were normally arranged. Compared with those in p^S/p^S, *st/st* individuals, the exocuticles of $p^S/+^{pS}$, *st/st* individuals were not evenly distributed (Figure 7A). Moreover, the cuticle thickness was slightly thicker than those of $+^p+^p$, *st/st* individuals. (Figure 7B). For the p^M/p^M, *st/st* individuals, the degree of melanism, density of melanin protrusions, and chitin

fiber arrangement was all similar to those of $p^{S}/+^{pS}$, *st/st* individuals (Figure 7A-7B). However, in $p^{M}/+^{pM}$, *st/st* individuals, the density of cuticle melanization and melanin protrusions was much less than that in the previously examined melanic individuals (Figure 7A). The exocuticle was damaged to some extent, but to a lower degree than that in $+^{p}+^{p}$, *st/st* individuals, and the cuticle thickness was close to that in the $+^{p}+^{p}$, *st/st* individuals (Figure 7A-7B).

Gene expression analysis indicated that the transcript levels of *BmCPR2* in $p^{B}/+^{pB}$, *st/st* individuals were lower than those in $p^{B}/+^{pB}$, $+^{st}/st$ individuals (owing to the effects non-sense mediated decay), whereas the expression levels of other three *BmLcps* did not differ between $p^{B}/+^{pB}$, $+^{st}/st$ and $p^{B}/+^{pB}$, *st/st* individuals (Figure 7C). However, the darker body color and the expression of cuticular protein-encoding genes in p^{S}/p^{S}, *st/st* individuals was higher than that in $p^{S}/+^{pS}$, *st/st* individuals (Figure. 7C). A similar result was also obtained from the p^{M}/p^{M}, *st/st* and $p^{M}/+^{pM}$, *st/st* individuals (Figure 7C). In comparison with p^{M}/p^{M}, *st/st* and $p^{S}/+^{pS}$, *st/st* genotyped individuals, which had similar body shape characteristics, *BmCPR2* and *BmLcp18* were expressed at higher levels in p^{M}/p^{M}, *st/st* individuals than in $p^{S}/+^{pS}$, *st/st* individuals. *BmLcp22* and *BmLcp30* were expressed at higher levels in $p^{S}/+^{pS}$, *st/st* individuals than in p^{M}/p^{M}, *st/st* individuals (Figure 7C).

4. Discussion

In the 4th molting stage of *Bombyx mori*, the new cuticle layer forms approximately 16 h during the 4th molting period, and melanin deposition in the stripe begins 24 h during the 4th molting period (Tao-Jun-Feng et al., 2014). In *Papilio* larvae, the melanin in the stripe is also deposited at the late molting stage (Futahashi et al., 2010; Futahashi and Fujiwara). In

our results, the cuticular sections showed that melanin was deposited primarily in the epicuticle region, which is involved in the melanic region of *stony* mutants and WT or other melanic mutant strains. The surface physical characteristics of the melanic cuticle regions (Fig. S3A) were similar to those previously reported (Futahashi et al., 2012; He et al., 2016; Jan et al., 2017; Tan et al., 2016). Variations in chitin content (Fig. S3B) have also been shown to be associated with cuticle melanism and expression patterns of cuticular protein-encoding genes (Balabanidou et al., 2019; Moussian et al., 2005; Moussian et al., 2006). Deposition of melanin was accompanied by thickening of the procuticle, which contained large amounts of chitin (Figure 1, Figure 5A). Regardless of the genotypes of the melanic mutants or the melanic markings in the non-melanic strains, excessive accumulation of melanin in the cuticle was tightly associated with particular cuticular physical characteristics. We speculate that this phenomenon may be beneficial in maintaining the physiological function of the melanic cuticle. The significant differences in cuticular physical features between melanic and non-melanic integument regions provide clear evidence of the effects of melanism on cuticle characteristics.

Excessive accumulation of melanin was tightly associated with significantly up-regulated expression of melanin synthase genes (Fig. S8). The up-regulation of these four genes encoding larval cuticular proteins in melanic integuments was independent of genetic background (Figure 2 and 3, Fig. S4) (Futahashi et al., 2012; He et al., 2016; Jan et al., 2017; Wu et al., 2016). For other cuticular protein-encoding genes, even some predominantly expressed in non-larval stages (Such as *BmCPG13* and *BmCPR68*) (Xia et al., 2007), their expression was still up-regulated in the melanic integument regions (Fig. S8). These results

suggested that this correlation is universal. In contrast, the up-regulation of cuticular protein-encoding genes did not affect cuticle melanism (Tajiri, 2017; Xiong et al., 2017). The degree of melanism in stripes in the *stony* mutant was less than that in the WT (Fig. S9). The comparison of stripes between $p^{S}/+^{pS}$, $+^{st}/+^{st}$ and $p^{S}/+^{pS}$, *st*/*st* individuals also showed similar results (Figure 3A, Figure 6A). Thus, we speculate that *BmCPR2* is also involved in maintaining the cuticular coloring pattern. Previous studies have also reported the importance of larval cuticular protein-encoding genes in maintaining the melanic body color of larvae (Xiong et al., 2017). Additionally, structural characteristics of different cuticular layers are not produced independently: mutations affecting one protein located in a certain cuticular layer also affect the structures of other cuticular layers (Mun et al., 2019; Sobala and Adler, 2016). Therefore, we considered that during cuticle development, when the melanism-promoting signals occur, the up-regulation of *BmCPR2*, *BmLcp18*, *BmLcp22*, and *BmLcp30* may be a necessary adaptation enabling the dynamic process of excess melanin deposition, and the maintenance and stability of the structural characteristics and physical properties of melanic cuticles. In further research, detecting the dynamic changes in melanin deposition and the distribution of cuticular proteins in detail would contribute to exploration of the interactions among major cuticle components.

The variations in expression of certain cuticular protein-encoding genes did not affect other members (Fig. S5 and S6), in agreement with findings in other reports (Arakane et al., 2012; Noh et al., 2015; Xiong et al., 2017). These results indicate that there is no direct regulation of expression between larval cuticular protein-encoding genes with similar expression and function. Moreover, to our knowledge, there is no evidence suggesting that cuticular proteins

441 can enter the nucleus and regulate gene expression by acting as transcription factors.
442 Extensive accumulation of melanin precursors in epidermal cells is essential for cuticle
443 melanization; thus, melanism promotes the expression of cuticular protein-encoding genes, a
444 process driven by coordination between the accumulation of melanin precursors and the
445 expression of cuticular protein-encoding genes. Our results demonstrated that changes in
446 intracellular melanin precursors are important for regulating the expression of cuticular
447 protein-encoding genes (Figure 4, Figure 5). Some evidence also supports that melanin
448 precursors can regulate gene expression through the receptors of melanin precursors (Berke et
449 al., 1998; Konradi et al., 1996; Westin et al., 2001). Furthermore, BH_4 and DAHP affect the
450 synthesis of melanin precursors, thus leading to coordinated variations in the expression of
451 cuticular proteins; however, these two chemicals do not directly impair the extracellular
452 accumulation of melanin or protein-protein interactions in the cuticle. More importantly,
453 treatment introducing melanin precursor into non-melanic integuments results in a melanic
454 cuticular phenotype and up-regulated expression of four larval cuticular protein-encoding
455 genes (Figure 5); these results establish a direct relationship between melanin precursors and
456 larval cuticular protein-encoding genes. We believe that up-regulation of *BmCPR2*, *BmLcp18*,
457 *BmLcp22*, and *BmLcp30* may have occurred simultaneously, owing to excessive amounts of
458 melanin precursors, but these four RR1-type *BmLcps* are not expected to be mutually
459 regulated. Notably, several studies have found that mutations in genes affecting melanin
460 synthesis or regulation influence not only the pigmentation but also the morphology and
461 structure of the cuticle (Concha et al., 2019; Massey et al., 2019; Matsuoka and Monteiro,
462 2017; Mun et al., 2019). These genes are directly or indirectly involved in the synthesis and

463 accumulation of melanin precursors. From the perspective of the effects on cuticle
464 characteristics, variations in melanin precursor content should be closely associated with
465 changes in cuticular structure. Thus, we suggest that the regulation of cuticular protein-genes
466 by melanin precursors may lie at the core of this association. Further analyses will be
467 performed to explore the response elements in the regulatory sequences of *BmLcp* genes and
468 to determine the detailed molecular mechanisms of melanin precursors.

469 Although there are 148 RR-type cuticular proteins in the silkworm genome (Futahashi et al.,
470 2008), RR1-type *BmLcp* genes were chosen on the basis of their similar expression patterns
471 (Fig. S1) and chitin-binding characteristics during larval development (Dong et al., 2016;
472 Liang et al., 2010; Nakato et al., 1994; Nakato et al., 1997; Okamoto et al., 2008; Qiao et al.,
473 2014; Tang et al., 2010; Xiong et al., 2017). Additionally, the near isogenic line Dazao-*stony*
474 was almost genetically and phenotypically identical to the wild-type Dazao strain with
475 *BmCPR2* knockout (Qiao et al., 2014). We cannot exclude the possibility that other cuticular
476 protein-encoding genes (up-regulated under melanic cuticle regions) might participate in
477 maintaining the structure of the melanic cuticle. We focused on these four RR1-type *BmLcps*
478 as typical representatives, to enable specific analysis of the compensatory effects and the
479 relevant phenotypic cuticular characteristics under the larval developmental stages and
480 conditions. In follow-up research, we will introduce a melanism background into lines with
481 knockout of the other three cuticular protein-encoding genes (*BmLcp18*, *BmLcp22*, and
482 *BmLcp30*) to verify the complementarity effect hypothesis.

483 Because homozygous p^B mutations are lethal (Banno et al., 2005; Xiang, 1995), we were
484 unable to obtain F_2 progeny with the p^B/p^B, *st/st* genotype. However, individuals with the

485 $p^B/+^{pB}$, $+^{st}/st$ and $p^B/+^{pB}$, *st/st* genotypes had almost the same body shape and degree of
486 melanism (Figure 6A). In the back-cross progeny of p^B×*stony*, the observed number of
487 individuals with p^B-type melanism and normal body shape was twice that expected (Figure 6A
488 and 6B, Table 1, Table 4). Among these individuals, 25% of $p^B/+^{pB}$, *st*/*st* individuals were
489 suspected to have p^B-type melanic cuticles and a *stony*-type body shape, but this phenotype
490 was not observed (Figure 6A and 6B, Table 1, Table 4). This result may be explained by the
491 epistatic effect of excessive melanism on the *stony*-type body shape phenotype. Similarly, in
492 the progeny of p^S×*stony*, an additional 1/16 of individuals had a p^S-type color pattern and
493 normal body shape, a proportion greater than expected (theoretical ratio, 9:16); moreover,
494 approximately 1/16 of individuals had the p^S/p^S, *st*/*st* genotype (theoretically, they should have
495 had a p^S-type color pattern with a typical *stony*-type body shape) (Figure 6A and 6B, Table 2,
496 Table 4). In addition, 1.740/16 of $p^S/+^{pS}$, *st*/*st* individuals (close to 2/16) with light melanic
497 color were practically masked cuticular defects, and therefore most of them exhibited the
498 ambiguous *stony*-like body shape (approximately 0.097/16 individuals with the genotype
499 $p^S/+p^S$, *st*/*st* had normal body shape and therefore were not included in the calculation)
500 (Figure 6A and 6B, Table 2, Table 4). The sum of the proportions of p^S/p^S, *st*/*st* individuals to
501 $p^S/+^{pS}$, *st/st* individuals (2.804/16) was very close to the expected value of 3/16 for $p^S/\_$, *st*/*st*
502 individuals (Table 2, Table 4). Moreover, the ratio deviation of the genotype and phenotype of
503 p^M×*stony* progeny was similar to that of p^S×*stony* progeny (Figure 6A and 6B, Table 3, Table
504 4). The proportion of $p^B/+^{pB}$, *st/st* (ratio = 1.027:4), *ps*/$+^{pS}$, *st/st* (ratio = 1.837:16), and $p^M/+^{pM}$,
505 *st/st* (ratio = 1.940:16) genotyped individuals was close to the expected value (1:4, 2:16, and
506 2:16, respectively) (Tables 1–4). The different degrees of melanism with a homozygous or

heterozygous *p* locus led to different levels of epistatic effects (Figure 6, Figure 7, Tables 1–4). These phenotypes were completely or partially masked by melanism (Figure 6; Tables 1–4). These characteristics further validate the masking effect of melanism on defective body shape at the molecular level. Considering the phenotypic characteristics, cuticular section structure, and expression of cuticular protein-encoding genes in the progeny with melanic color and the *st/st* genotype, we suggest that the epistatic effect may be due to up-regulation of cuticular protein-encoding genes under a melanism background, thereby resulting in accumulation of more cuticular proteins with similar functions in the cuticle and masking the cuticular defects in *st/st* individuals. The degree of compensation was in the order $p^{B}/+^{pB}$, *st/st* > p^{S}/p^{S}, *st/st* > (p^{M}/p^{M}, *st/st* or $p^{S}/+^{pS}$, *st/st*) > $p^{M}/+^{pM}$, *st/st*, which corresponds well to the gradual decrease in the degree of melanism (Figure 6, Figure 7, Tables 1–4). The compensatory effects of melanic body color on defective cuticular features also provided new evidence explaining how melanism can be a beneficial trait (Liu et al., 2015b; Mallet and Hoekstra, 2016; True, 2003; Wilson et al., 2001; Wittkopp and Beldade, 2009; Wittkopp et al., 2003).

On the basis of our results, we propose the following model to explain our findings: 1) the larval cuticular protein-encoding genes *BmCPR2*, *BmLcp18*, *BmLcp22*, and *BmLcp30* are up-regulated by the induction of accumulated melanin precursors, and their expression levels are positively correlated with the degree of melanism; this induction pattern ensures the formation of normal structural features of the melanic cuticle; 2) if a melanism background is introduced into *BmCPR2* deleted individuals through a genetic cross, other cuticular protein genes with similar functions, *BmLcp18*, *BmLcp22*, and *BmLcp30* (induced by melanin precursors), can compensate for the morphological and adaptive defects caused by

dysfunctional *BmCPR2*; the degree of compensation increases with the accumulation of melanin (Figure 8). Because excess melanin and cuticular proteins commonly occur together in other insects (Andersen, 2010; Cohen and Moussian, 2016; Moussian, 2010), and homologues of the four RR1-type BmLcps are widely distributed in Lepidoptera (Table S2), we presume that the induction phenomenon, as well as its corresponding biological importance might be conserved in Lepidoptera.

References

Andersen, S.O., 2010. Insect cuticular sclerotization: a review. Insect Biochem Mol Biol 40, 166-178.

Arakane, Y., Lomakin, J., Gehrke, S.H., Hiromasa, Y., Tomich, J.M., Muthukrishnan, S., Beeman, R.W., Kramer, K.J., Kanost, M.R., 2012. Formation of rigid, non-flight forewings (elytra) of a beetle requires two major cuticular proteins. PLoS Genet 8, e1002682.

Balabanidou, V., Kefi, M., Aivaliotis, M., Koidou, V., Girotti, J.R., Mijailovsky, S.J., Juárez, M.P., Papadogiorgaki, E., Chalepakis, G., Kampouraki, A., Nikolaou, C., Ranson, H., Vontas, J., 2019. Mosquitoes cloak their legs to resist insecticides. Proceedings of the Royal Society B: Biological Sciences 286, 20191091.

Banno, Y., Fujii, H., Kawaguchi, Y., Yamamoto, K., Nishikawa, K., Nishisaka, A., Tamura, K., Eguchi, S., 2005. A guide to the silkworm mutants: 2005 gene name and gene symbol. Kyusyu University, Fukuoka, Japan.

Berke, J.D., Paletzki, R.F., Aronson, G.J., Hyman, S.E., Gerfen, C.R., 1998. A complex program of striatal gene expression induced by dopaminergic stimulation. J Neurosci 18, 5301-5310.

Chaudhari, S.S., Arakane, Y., Specht, C.A., Moussian, B., Boyle, D.L., Park, Y., Kramer, K.J., Beeman, R.W., Muthukrishnan, S., 2011. Knickkopf protein protects and organizes chitin in the newly synthesized insect exoskeleton. P Natl Acad Sci USA 108, 17028-17033.

Cohen, E., Moussian, B., 2016. Extracellular Composite Matrices in Arthropods. Springer, Switzerland.

Concha, C., Wallbank, R.W.R., Hanly, J.J., Fenner, J., Livraghi, L., Rivera, E.S., Paulo, D.F., Arias, C., Vargas, M., Sanjeev, M., Morrison, C., Tian, D., Aguirre, P., Ferrara, S., Foley, J., Pardo-Diaz, C., Salazar, C., Linares, M., Massardo, D., Counterman, B.A., Scott, M.J., Jiggins, C.D., Papa, R., Martin, A., McMillan, W.O., 2019. Interplay between Developmental Flexibility and Determinism in the Evolution of Mimetic Heliconius Wing Patterns. Current Biology 29, 3996-4009.e3994.

Dai, F., Lu, C., Xiang, Z., 2000. A study on the genetics of "new stony"-a natural mutant in silkworm. Acta Sericologica Sinica 26, 53-55.

Delgado-Esteban, M., Almeida, A., Medina, J.M., 2002. Tetrahydrobiopterin deficiency increases neuronal vulnerability to hypoxia. J Neurochem 82, 1148-1159.

Dong, Z., Zhang, W., Zhang, Y., Zhang, X., Zhao, P., Xia, Q., 2016. Identification and Characterization of Novel Chitin-Binding Proteins from the Larval Cuticle of Silkworm, Bombyx mori. J Proteome Res

15, 1435-1445.
Fujii, T., Abe, H., Kawamoto, M., Katsuma, S., Banno, Y., Shimada, T., 2013. Albino (al) is a tetrahydrobiopterin (BH_4)-deficient mutant of the silkworm *Bombyx mori*. Insect Biochem Mol Biol 43, 594-600.
Futahashi, R., Banno, Y., Fujiwara, H., 2010. Caterpillar color patterns are determined by a two□phase melanin gene prepatterning process: new evidence from tan and laccase2. Evolution & Development 12.
Futahashi, R., Fujiwara, H., Melanin-synthesis enzymes coregulate stage-specific larval cuticular markings in the swallowtail butterfly,Papilio xuthus. 215, 519-529.
Futahashi, R., Fujiwara, H., 2005. Melanin-synthesis enzymes coregulate stage-specific larval cuticular markings in the swallowtail butterfly, *Papilio xuthus*. Dev Genes Evol 215, 519-529.
Futahashi, R., Fujiwara, H., 2006. Expression of one isoform of GTP cyclohydrolase I coincides with the larval black markings of the swallowtail butterfly, Papilio xuthus. Insect Biochemistry and Molecular Biology 36, 63-70.
Futahashi, R., Okamoto, S., Kawasaki, H., Zhong, Y.S., Iwanaga, M., Mita, K., Fujiwara, H., 2008. Genome-wide identification of cuticular protein genes in the silkworm, Bombyx mori. Insect Biochem Mol Biol 38, 1138-1146.
Futahashi, R., Shirataki, H., Narita, T., Mita, K., Fujiwara, H., 2012. Comprehensive microarray-based analysis for stage-specific larval camouflage pattern-associated genes in the swallowtail butterfly, *Papilio xuthus*. BMC Biol 10, 46.
Guan, X., Middlebrooks, B.W., Alexander, S., Wasserman, S.A., 2006. Mutation of TweedleD, a member of an unconventional cuticle protein family, alters body shape in *Drosophila*. P Natl Acad Sci USA 103, 16794-16799.
He, S.Z., Tong, X.L., Lu, K.P., Lu, Y.R., Luo, J.W., Yang, W.H., Chen, M., Han, M.J., Hu, H., Lu, C., Dai, F.Y., 2016. Comparative analysis of transcriptomes among *Bombyx mori* strains and sexes reveals the genes regulating melanic morph and the related phenotypes. Plos One 11.
Hopkins, T.L., Kramer, K.J., 1992. Insect cuticle sclerotization. Annu rev entomol 37, 273-302.
Hu, F., Zhang, G.N., Wang, J.J., 2009. Scanning electron microscopy studies of antennal sensilla of bruchid beetles, Callosobruchus chinensis (L.) and Callosobruchus maculatus (F.) (Coleoptera: Bruchidae). Micron 40, 320-326.
Hu, Y.G., Shen, Y.H., Zhang, Z., Shi, G.Q., 2013. Melanin and urate act to prevent ultraviolet damage in the integument of the silkworm, Bombyx mori. Arch Insect Biochem Physiol 83, 41-55.
Jan, S., Li, C., Liu, S., Liu, X., Zhu, F., Hafeez, M., Wang, M., 2017. Microscopic cuticle structure comparison of pupal melanic and wild strain of Spodoptera exigua and their gene expression profiles in three time points. Microb Pathog.
Kanekatsu, R., Banno, Y., Nagashima, E., Miyashita, T., 1988. Genetical studies on a new spontaneous mutant "Bamboo" (*Bo*) of the silkworm. The Journal of Sericultural Science of Japan 57, 151-156.
Konradi, C., Leveque, J.C., Hyman, S.E., 1996. Amphetamine and dopamine-induced immediate early gene expression in striatal neurons depends on postsynaptic NMDA receptors and calcium. J Neurosci 16, 4231-4239.
Liang, J., Zhang, L., Xiang, Z., He, N., 2010. Expression profile of cuticular genes of silkworm, *Bombyx mori*. BMC Genomics 11, 173.
Liu, S., Wang, M., Li, X., 2015a. Pupal melanization is associated with higher fitness in Spodoptera exigua. Scientific reports 5.

Liu, S.S., Wang, M., Li, X.C., 2015b. Pupal melanization is associated with higher fitness in *Spodoptera exigua*. Sci Rep-Uk 5.

Mallet, J., Hoekstra, H.E., 2016. Ecological genetics: a key gene for mimicry and melanism. Curr Biol 26, R802-R804.

Massey, J.H., Chung, D., Siwanowicz, I., Stern, D.L., Wittkopp, P.J., 2019. The yellow gene influences Drosophila male mating success through sex comb melanization. eLife 8, e49388.

Matsuoka, Y., Monteiro, A., 2017. Melanin pathway genes regulate color and morphology of butterfly wing scales. Mechanisms of Development.

Min, C., Song, J.B., Zhi-Quan, L.I., Tang, D.M., Tong, X.L., Dai, F.Y., 2016. Progress and perspective of silkworm as a model of human diseases for drug screening. Acta Pharmaceutica Sinica.

Mitchell, B.M., Dorrance, A.M., Webb, R.C., 2003. GTP cyclohydrolase 1 inhibition attenuates vasodilation and increases blood pressure in rats. Am J Physiol Heart Circ Physiol 285, H2165-2170.

Moussian, B., 2010. Recent advances in understanding mechanisms of insect cuticle differentiation. Insect Biochem Mol Biol 40, 363-375.

Moussian, B., Schwarz, H., Bartoszewski, S., Nusslein-Volhard, C., 2005. Involvement of chitin in exoskeleton morphogenesis in *Drosophila melanogaster*. J Morphol 264, 117-130.

Moussian, B., Tang, E., Tonning, A., Helms, S., Schwarz, H., Nusslein-Volhard, C., Uv, A.E., 2006. Drosophila Knickkopf and Retroactive are needed for epithelial tube growth and cuticle differentiation through their specific requirement for chitin filament organization. Development 133, 163-171.

Mun, S., Noh, M.Y., Kramer, K.J., Muthukrishnan, S., Arakane, Y., 2019. Gene functions in adult cuticle pigmentation of the yellow mealworm, Tenebrio molitor. Insect Biochem Molec, 103291.

Nakato, H., Shofuda, K., Izumi, S., Tomino, S., 1994. Structure and developmental expression of a larval cuticle protein gene of the silkworm, Bombyx mori. Biochim Biophys Acta 1218, 64-74.

Nakato, H., Takekoshi, M., Togawa, T., Izumi, S., Tomino, S., 1997. Purification and cDNA cloning of evolutionally conserved larval cuticle proteins of the silkworm, Bombyx mori. Insect Biochem Mol Biol 27, 701-709.

Noh, M.Y., Muthukrishnan, S., Kramer, K.J., Arakane, Y., 2015. *Tribolium castaneum* RR-1 cuticular protein TcCPR4 is required for formation of pore canals in rigid cuticle. PLoS Genet 11.

Noh, M.Y., Muthukrishnan, S., Kramer, K.J., Arakane, Y., 2016. Cuticle formation and pigmentation in beetles. Curr Opin Insect Sci 17, 1-9.

Okamoto, S., Futahashi, R., Kojima, T., Mita, K., Fujiwara, H., 2008. Catalogue of epidermal genes: genes expressed in the epidermis during larval molt of the silkworm *Bombyx mori*. BMC Genomics 9, 396.

Oota, K., Kanekatsu, R., 1993. Morphological studies on the Bamboo (*Bo*) mutant of the silkworm, *Bombyx mori*. The Journal of Sericultural Science of Japan 62, 448-454.

Qiao, L., Xiong, G., Wang, R.X., He, S.Z., Chen, J., Tong, X.L., Hu, H., Li, C.L., Gai, T.T., Xin, Y.Q., Liu, X.F., Chen, B., Xiang, Z.H., Lu, C., Dai, F.Y., 2014. Mutation of a cuticular protein, BmorCPR2, alters larval body shape and adaptability in silkworm, Bombyx mori. Genetics 196, 1103-1115.

Shofuda, K., Togawa, T., Nakato, H., Tomino, S., Izumi, S., 1999. Molecular cloning and characterization of a cDNA encoding a larval cuticle protein of Bombyx mori. Comp Biochem Physiol B Biochem Mol Biol 122, 105-109.

Sobala, L.F., Adler, P.N., 2016. The Gene Expression Program for the Formation of Wing Cuticle in Drosophila. PLOS Genetics 12, e1006100.

Suderman, R.J., Dittmer, N.T., Kanost, M.R., Kramer, K.J., 2006. Model reactions for insect cuticle

sclerotization: cross-linking of recombinant cuticular proteins upon their laccase-catalyzed oxidative conjugation with catechols. Insect Biochem Mol Biol 36, 610-611.

Tajiri, R., 2017. Cuticle itself as a central and dynamic player in shaping cuticle. Curr Opin Insect Sci 19, 30-35.

Tan, D., Tong, X.L., Hu, H., Wu, S.Y., Li, C.L., Xiong, G., Xiang, Z.H., Dai, F.Y., Lu, C., 2016. Morphological characterization and molecular mapping of an irradiation-induced Speckled mutant in the silkworm, *Bombyx mori*. Insect Mol Biol 25, 93-104.

Tang, L., Liang, J., Zhan, Z., Xiang, Z., He, N., 2010. Identification of the chitin-binding proteins from the larval proteins of silkworm, Bombyx mori. Insect Biochem Mol Biol 40, 228-234.

Tao-Jun-Feng, S.U., Xia, C.L., Yan-Jun, L.I., Zhang, X.Y., Zhou, M.T., Zhang, Y.X., Liu, C., Xia, Q.Y., 2014. Anatomical Observation of Melanin Formation in Markings on Integuments of Bombyx mori. Science of Sericulture.

Tong, X., Liang, P., Wu, S., Li, Y., Qiao, L., Hu, H., Xiang, Z., Lu, C., Dai, F., 2018. Disruption of PTPS Gene Causing Pale Body Color and Lethal Phenotype in the Silkworm, Bombyx mori. Int J Mol Sci 19.

True, J.R., 2003. Insect melanism: the molecules matter. Trends Ecol Evol 18, 640-647.

Van Belleghem, S.M., Rastas, P., Papanicolaou, A., Martin, S.H., Arias, C.F., Supple, M.A., Hanly, J.J., Mallet, J., Lewis, J.J., Hines, H.M., Ruiz, M., Salazar, C., Linares, M., Moreira, G.R.P., Jiggins, C.D., Counterman, B.A., McMillan, W.O., Papa, R., 2017. Complex modular architecture around a simple toolkit of wing pattern genes. Nat Ecol Evol 1.

Westin, J.E., Andersson, M., Lundblad, M., Cenci, M.A., 2001. Persistent changes in striatal gene expression induced by long-term L-DOPA treatment in a rat model of Parkinson's disease. Eur J Neurosci 14, 1171-1176.

Wilson, K., Cotter, S.C., Reeson, A.F., Pell, J.K., 2001. Melanism and disease resistance in insects. Ecol Lett 4, 637-649.

Wittkopp, P.J., Beldade, P., 2009. Development and evolution of insect pigmentation: genetic mechanisms and the potential consequences of pleiotropy. Semin Cell Dev Biol 20, 65-71.

Wittkopp, P.J., Carroll, S.B., Kopp, A., 2003. Evolution in black and white: genetic control of pigment patterns in *Drosophila*. Trends Genet 19, 495-504.

Wu, S.Y., Tong, X.L., Peng, C.X., Xiong, G., Lu, K.P., Hu, H., Tan, D., Li, C.L., Han, M.J., Lu, C., Dai, F.Y., 2016. Comparative analysis of the integument transcriptomes of the black dilute mutant and the wild-type silkworm *Bombyx mori*. Sci Rep-Uk 6.

Xia, Q., Cheng, D., Duan, J., Wang, G., Cheng, T., Zha, X., Liu, C., Zhao, P., Dai, F., Zhang, Z., He, N., Zhang, L., Xiang, Z., 2007. Microarray-based gene expression profiles in multiple tissues of the domesticated silkworm, Bombyx mori. Genome Biology 8, R162.

Xiang, Z., 1995. Genetics and Breeding of the Silkworm. CHN: Chinese Agriculture Press, Beijing.

Xiong, G., Tong, X., Gai, T., Li, C., Qiao, L., Monteiro, A., Hu, H., Han, M., Ding, X., Wu, S., Xiang, Z., Lu, C., Dai, F., 2017. Body Shape and Coloration of Silkworm Larvae Are Influenced by a Novel Cuticular Protein. Genetics 207, 1053-1066.

Yoda, S., Yamaguchi, J., Mita, K., Yamamoto, K., Banno, Y., Ando, T., Daimon, T., Fujiwara, H., 2014. The transcription factor Apontic-like controls diverse colouration pattern in caterpillars. Nat Commun 5, 4936.

Zhang, J., Zhu, K.Y., 2006. Characterization of a chitin synthase cDNA and its increased mRNA level associated with decreased chitin synthesis in Anopheles quadrimaculatus exposed to diflubenzuron.

Insect Biochem Mol Biol 36, 712-725.

Acknowledgments

We thank Dr. Wei Sun, Dr. Tianzhu Xiong, Dr. Minjin Han, Dr. Chunlin Li, Dr. Yonggang Hu, Dr. Kunpeng Lu, and Dr. Yaqun Xin for providing valuable advice. This work was supported by the National Natural Science Foundation of China (Nos. 31830094, 31772527), the Hi-Tech Research and Development 863 Program of China (grant No. 2013AA102507), the Natural Science Foundation Project of ChongQing (CSTC) (No. cstc2017jcyjAX0023), the Open Foundation of The State Key Laboratory of Silkworm Genome Biology (SKLSGB1819-6), the Bayu young scholars program, the Scientific and Technological Research Program of the Chongqing Municipal Education Commission (KJQN201900523), and the China Agriculture Research System (No. CARS-18-ZJ0102).

Author contribution

LQ and FYD conceived and coordinated the study and wrote the paper. LQ and FYD designed the experiments. LQ, ZWY, RXW, GX, HH, SZH, and JBS performed the experiments. LQ, GX, YJH, and XLT analyzed the data. LQ, JM, LRC, BC, and CL revised the paper. All authors read and approved the final manuscript.

Figure legends

Figure 1. Comparison of the physical structure between melanic and non-melanic cuticle. A. Cross-section of cuticle from the same integument areas in Dazao, Dazao-*stony*, and p^{S}. Scale bar = 10 μm. Epi: epicuticle, exo: exocuticle, endo: endocuticle, pro: procuticle. The

720 disordered arrangements in the procuticle of Dazao-*stony* are boxed in red. Red arrows
721 indicate damage to the exocuticle in Dazao-*stony*. B. Thickness of cuticles in Figure A.
722 One-way ANOVA test, n = 3, F = 47.36, n = 3, $p < 0.05$.

723

724 Figure 2. Expression of *BmCPR2*, *BmLcp18*, *BmLcp22*, and *BmLcp30* in melanic and
725 non-melanic integuments. A and B show relative gene expression levels in the semi-lunar
726 marking (black box) and the non-melanic region (between the semi-lunar marking, red box)
727 in Dazao and Dazao-*stony* strains. Scale bar is 2 mm. C shows a comparative analysis of
728 relative gene expression levels at the dorsal side of abdominal segments (from the third to the
729 fourth segment, red box) in p^S and Dazao strains. Scale bar is 1 cm. D shows a comparison of
730 relative gene expression levels between the 2nd instar *al* mutant and the Dazao strain (melanic).
731 The red hash tag symbol indicates that the Fig. 1 D shown here is from a previous study from
732 our group (Min et al., 2016) with modifications. Scale bar is 2 mm. n = 3, *t*-test, asterisks
733 denote statistical significance, * $p < 0.05$; ** $p < 0.01$; *** $p < 0.001$.

734

735 Figure 3. Expression of cuticular protein-encoding genes in integuments with different
736 degrees of melanism. A. Comparison of melanism degree. One-way ANOVA test, n = 6, F =
737 290.6, $p < 0.0001$. B. Gene expression levels of cuticular protein-encoding genes among four
738 strains with mutant alleles at the *p* locus ($+^p$, p^M, p^S, and p^B). Scale bar is 1 cm. Ratios
739 represent the ratios of gene expression levels between two strains. Symbols (−, +, ++, and
740 +++) represent the degree of melanism. Stars represent melanin-associated cuticular
741 protein-encoding genes. *t*-test, n = 3, asterisks denote statistical significance, * $p < 0.05$; ** $p <$

742 0.01.

743

744 Figure 4. Effects of melanin precursors (Figure 6A, in *BmE* cells) and BH_4 (Figure 6B and 6C,
745 in *vivo*) on the expression of cuticular protein-encoding genes. *t*-test, n = 3, asterisks denote
746 statistical significance, * $p < 0.05$; ** $p < 0.01$.

747

748 Figure 5. Effects of treatment with melanin precursors on cuticle pigmentation and expression
749 of cuticular protein-encoding genes. A. Cuticle pigmentation in the melanin precursor treated
750 group and control group. Scale bar = 2 mm. The melanic regions are marked with arrows and
751 rectangles. B. Gene expression analysis in L-Dopa and dopamine treated groups and the
752 control group. *t*-test, n = 3, asterisks denote statistical significance, ** $p < 0.01$.

753

754 Figure 6. Association analysis of the genotypes and phenotypes in segregated progeny from
755 different crosses. A. Correlation analysis between the genotypes and phenotypes in
756 self-crossed or backcrossed progeny. Scale bar is 1 cm. White and red stars represent
757 polymorphic bands at the $+^{p}$ and melanic *p* locus (p^{M}, p^{S}, p^{B}), respectively. Red and white hash
758 tags represent polymorphic bands at the *st* and $+^{st}$ allele, respectively. Solid and dotted red
759 arrows indicate the relative degree of bulging (solid red arrows represent a higher degree of
760 bulging than that represented by the dotted red arrows). B. Ratios of the lengths of internodes
761 and intersegmental folds in the second, third, and fourth abdominal segments of individuals
762 with different genotypes for melanic body color, in the self-crossed or backcrossed progeny. n
763 ≥ 3, *t*-test, asterisks denote statistical significance, ** $p < 0.01$.

764

765 Figure 7. Features of the cuticle cross-section and gene expression patterns in *st/st* individuals
766 (progeny of BC_1 and F_2) under different melanic backgrounds. A. Features of the cuticle
767 cross-section in BC_1 and F_2 progeny with different degrees of melanism. Scale bar = 10 μm.
768 Epi: epicuticle, exo: exocuticle, endo: endocuticle, pro: procuticle. The disordered
769 arrangement in the procuticle is boxed in red. Red arrow represents damage to the exocuticle.
770 B. Cuticle thicknesses for all genotypes listed in Figure A. One-way ANOVA test, n = 3, F =
771 95.80, n = 3, $p < 0.05$. C. Expression analysis of cuticular protein-encoding genes in
772 heterozygotic individuals at the *p* locus from back-crossed progeny of $p^B \times$ *stony* and
773 expression analysis of cuticular protein-encoding genes in homozygotic and heterozygotic
774 individuals at the *p* locus from self-crossed progeny of $p^S \times$ *stony*, and $p^M \times$ *stony*, only if the
775 cuticle was melanic and the genotype was homozygous recessive at the *stony* locus. *t*-test, n =
776 3, asterisks denote statistical significance, * $p < 0.05$; ** $p \leq 0.01$.

777

778 Figure 8. Schematic overview of the effects of melanin precursors on the expression of
779 cuticular protein-encoding genes as well as larval body shape. Scale bar = 1 cm. In epidermal
780 cells, vertical black arrows indicate the increase in melanin precursor content, and the red
781 arrow indicates increased expression of larval cuticular protein-encoding genes (*Lcps*).
782 Asterisks represent similar expression patterns and functions of the *Lcps*. At the individual
783 level, the red backslash indicates partial deletion of the *BmCPR2* CDS sequence and
784 BmCPR2 dysfunction. Genes with similar expression patterns and functions to those of
785 *BmCPR2* are boxed; the red dotted arrow with red backslash indicates that the expression of

larval cuticular protein-encoding genes in the box was not up-regulated. The blue dotted arrow indicates that the boxed genes could not compensate for the deficiency caused by the function loss of BmCPR2. The red solid arrow indicates that the boxed genes were up-regulated under a melanism background. The blue solid arrow indicates that the boxed genes were able to compensate for the deficiency caused by the loss of BmCPR2 function.

Table 1. Segregation patterns of the phenotypes in the progeny from the (p^B×Dazao-*stony*) × Dazao-*stony* cross.

Phenotype	Expected Ratio	Possible Genotype	Observed Number	Observed Ratio
p^B-type color pattern, normal body shape	1:4	$p^B/+^{pB}$, $+^{st}/st$	290**	2.098: 4†
p^B-type color pattern, typical *stony*-type body shape	1:4	$p^B/+^{pB}$, *st/st*	0**	0:4†
non-melanic color pattern, normal body shape	1:4	$+^{pB}/+^{pB}$, $+^{st}/st$	138	0.998: 4
non-melanic color pattern, typical *stony*-type body shape	1:4	$+^{pB}/+^{pB}$, *st/st*	125	0.904: 4

** $p < 0.01$, chi-square test ($\chi^2 = 304.8$, df = 1); †Represents the actual modified Mendelian ratio.

Table 2. Segregation patterns of the phenotypes in the progeny from the p^S×Dazao-*stony* self-cross.

Phenotype	Expected Ratio	Possible Genotype	Observed Number	Observed Ratio
p^S-type color pattern, normal body shape	9:16	$p^S/\_$, $+^{st}/\_$	213**	10.296:16†
p^S-type color pattern, typical *stony*-type body shape	3:16	$p^S/\_$, *st/st*	0**	0:16†
non-melanic color pattern, normal body shape	3:16	$+^{pS}/+^{pS}$, $+^{st}/\_$	61	2.949:16
non-melanic color pattern, typical *stony*-type body shape	1:16	$+^{pS}/+^{pS}$, *st/st*	21	1.015:16
light p^S-type color pattern, ambiguous *stony*-like body shape+	0:16	$p^S/+^{pS}$, *st/st*^{a}	36	1.740:16

** $p < 0.01$, chi-square test ($\chi^2 = 65.9$, df = 1), numbers of "+" symbols represent the degree

of similarity of body shape to the *stony*-type body shape. † Represents the actual modified Mendelian ratio. Unexpected phenotypes in the observations are underlined. [a] Represents suspected $p^S/+^{pS}$,*st/st* genotype of individuals with a light p^S-type color pattern and an ambiguous *stony*-like body shape+.

Table 3. Segregation patterns of the phenotypes in the progeny from p^M×Dazao-*stony* self-cross.

Phenotype	Expected Ratio	Possible Genotype	Observed Number	Observed Ratio
p^M-type color pattern, normal body shape	9:16	$p^M/\_$, $+^{st}/\_$	275**	10.068:16†
p^M-type color pattern, typical *stony*-type body shape	3:16	$p^M/\_$, *st/st*	0**	0:16†
non-melanic color pattern, normal body shape	3:16	$+^{pM}/+^{pM}$, $+^{st}/\_$	84	3.076:16
non-melanic color pattern, typical *stony*-type body shape	1:16	$+^{pM}/+^{pM}$, *st/st*	27	0.989:16
very light p^M-type color pattern, ambiguous *stony*-like body shape+++	0:16	$^{pM}/+^{pM}$, *st/st*[a]	51	1.867:16†

** $p < 0.01$, chi-square test ($\chi^2 = 85.4$, df = 1, $p < 0.01$), numbers of "+" symbols represent the degree of similarity body shape to the *stony*-type body shape. † Represents the actual modified Mendelian ratio. Unexpected observed phenotypes are underlined. [a] Represents suspected $p^M/+^{pM}$,*st/st* genotype of individuals with a very light p^M-type color pattern and an ambiguous *stony*-like body shape+++.

Table 4. Actual genotyping of the melanic progeny from BC_1 and F_2 crosses involving *stony* and *p locus* alleles

Genotypes / Phenotypes	$p^B/+^{pB}$, $+^{st}/st$	$p^B/+^{pB}$, *st/st*	$p^S/\_$, $+^{st}/\_$	p^S/p^S, *st/st*	$p^S/+^{pS}$, *st/st*	$p^M/\_$, $+^{st}/\_$	p^M/p^M, *st/st*	$p^M/+^{pM}$, *st/st*
p^B-type color pattern, normal body shape	148 (148/553≈1.070:4)	142[a] (142/553≈1.027:4)	-	-	-	-	-	-
p^B-type color pattern, typical *stony*-type body shape	-	-	-	-	-	-	-	-
p^S-type color pattern, normal body shape	-	-	191 (191/331 ≈9.233/16)	20[b1] (20/331≈0.967/16)	2[b2] (0.097/16)	-	-	-
p^S-type color pattern, typical *stony*-type body shape	-	-	-	-	-	-	-	-

light p^S-type color pattern, ambiguous *stony*-like body shape+	-	-	-	-	36[b3] (36/331≈1.74/16)	-	-	-
p^M-type color pattern, normal body shape	-	-	-	-	-	244 (244/437≈8.934/16)	29[c1] (29/437≈1.062/16)	2[c2] (2/437≈0.073)
p^M-type color pattern, typical *stony*-type body shape	-	-	-	-	-	-	-	-
very light p^M-type color pattern, ambiguous *stony*-like body shape+++	-	-	-	-	-	-	-	51[c3] (51/437≈1.867/16)

[a] Indicates that the actual phenotype and expected phenotype of individuals with a $p^B/+^{pB}$, *st*/*st* genotype do not match, thus making the Mendelian separation ratio of the actual phenotype deviate significantly (see Table 1). The dotted arrow points to the expected phenotypic characteristics of this part of the genotype. [b1 b2] Indicate that among the individuals with a p^S-type color pattern and a normal body shape phenotype, there were approximately 0.967/16 p^S/p^S,*st*/*st* individuals and 0.097/16 $p^S/+^{pS}$,*st*/*st* individuals that did not have the expected phenotype, thus making the Mendelian segregation ratio of the actual phenotype significantly deviate from the expected phenotype (see Table 2). The dotted arrow points to the expected phenotypic characteristics of this part of the genotype. [b3] Indicates that the defective body shape of $p^S/+^{pS}$, *st*/*st* individuals (1.740/16) was partially masked by a light melanic body color. The dotted arrow points to the expected phenotypic characteristics of this part of the genotype. Individual aggregation, indicated by b1, b2, and b3, is the individual $p^S/\_$, *st*/*st* genotype, accounting for approximately 3/16 of the F_2 population. [c1 c2] Indicate that among the individuals with a p^M-type color pattern and a normal body shape phenotype, there were approximately 1.062/16 p^M/p^M,*st*/*st* individuals and 0.073/16 $p^M/+^{pM}$,*st*/*st* individuals that did not have the expected phenotype, thus making the Mendelian segregation ratio of the actual phenotype significantly deviate from the expected phenotype (see Table 3). The dotted arrow points to the expected phenotypic characteristics of this part of the genotype. [c3] Indicates that the defective body shape of $p^M/+^{pM}$, *st*/*st* genotyped individuals (1.867/16) was slightly masked by a very light melanic body color. Individual aggregation, indicated by c1, c2, and c3, is the individual $p^M/\_$, *st*/*st* genotype, accounting for approximately 3/16 of the F_2 population.

Figure 1

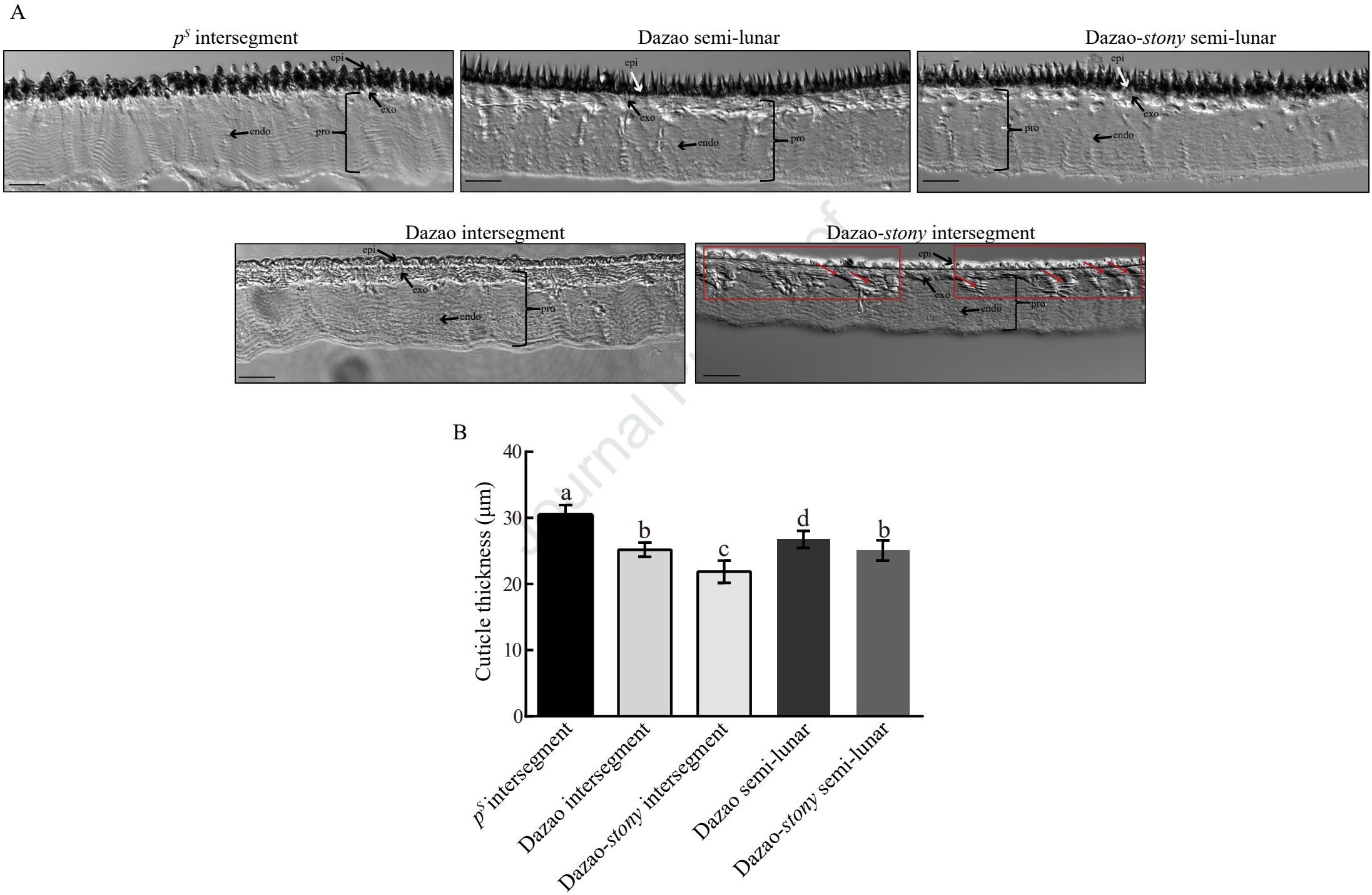
A
p^S intersegment
Dazao semi-lunar
Dazao-*stony* semi-lunar
Dazao intersegment
Dazao-*stony* intersegment
epi
exo
endo
pro
B
Cuticle thickness (μm)
0
10
20
30
40
a
b
c
d
b
p^S intersegment
Dazao intersegment
Dazao-*stony* intersegment
Dazao semi-lunar
Dazao-*stony* semi-lunar

Figure 2

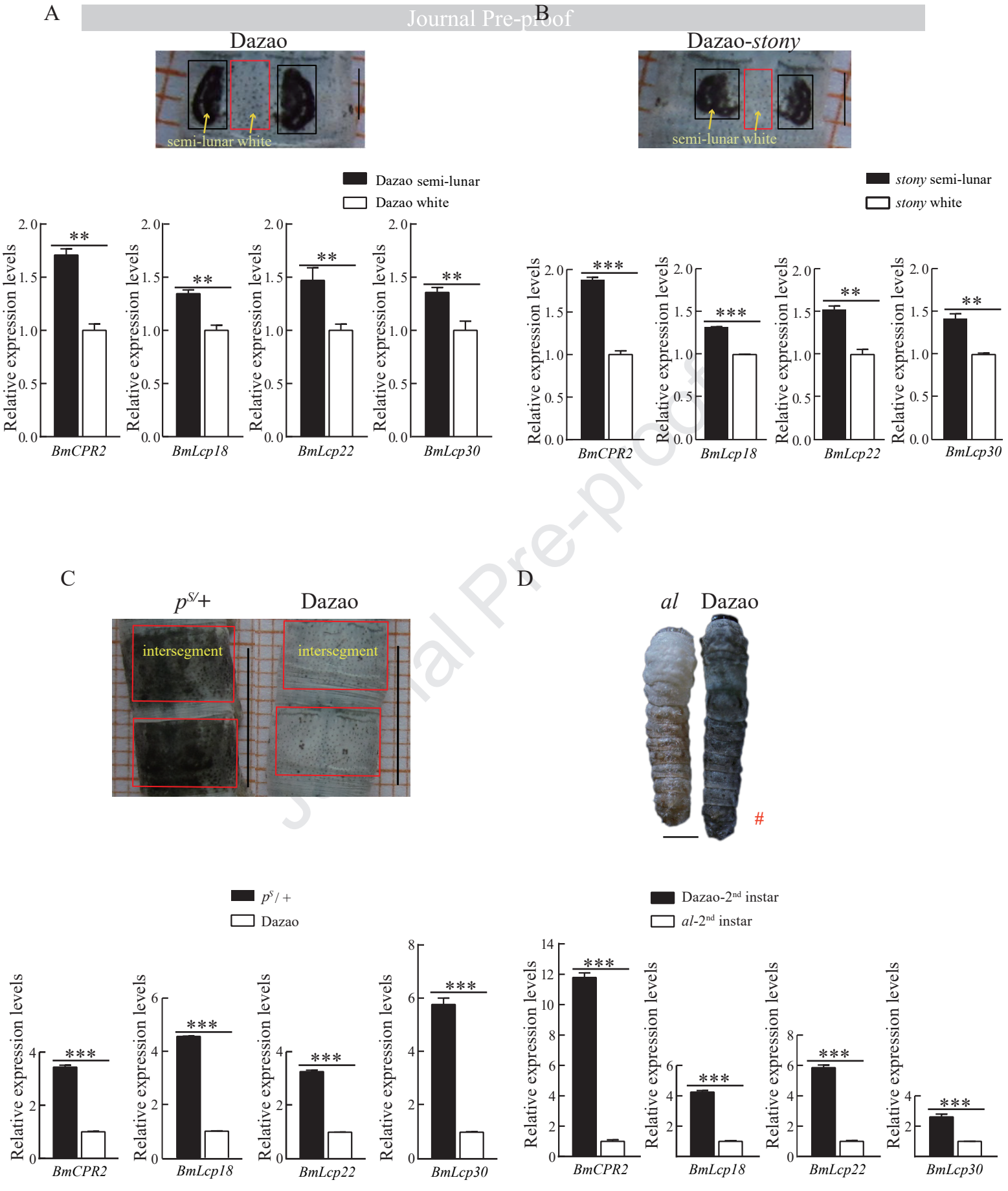

Figure 3

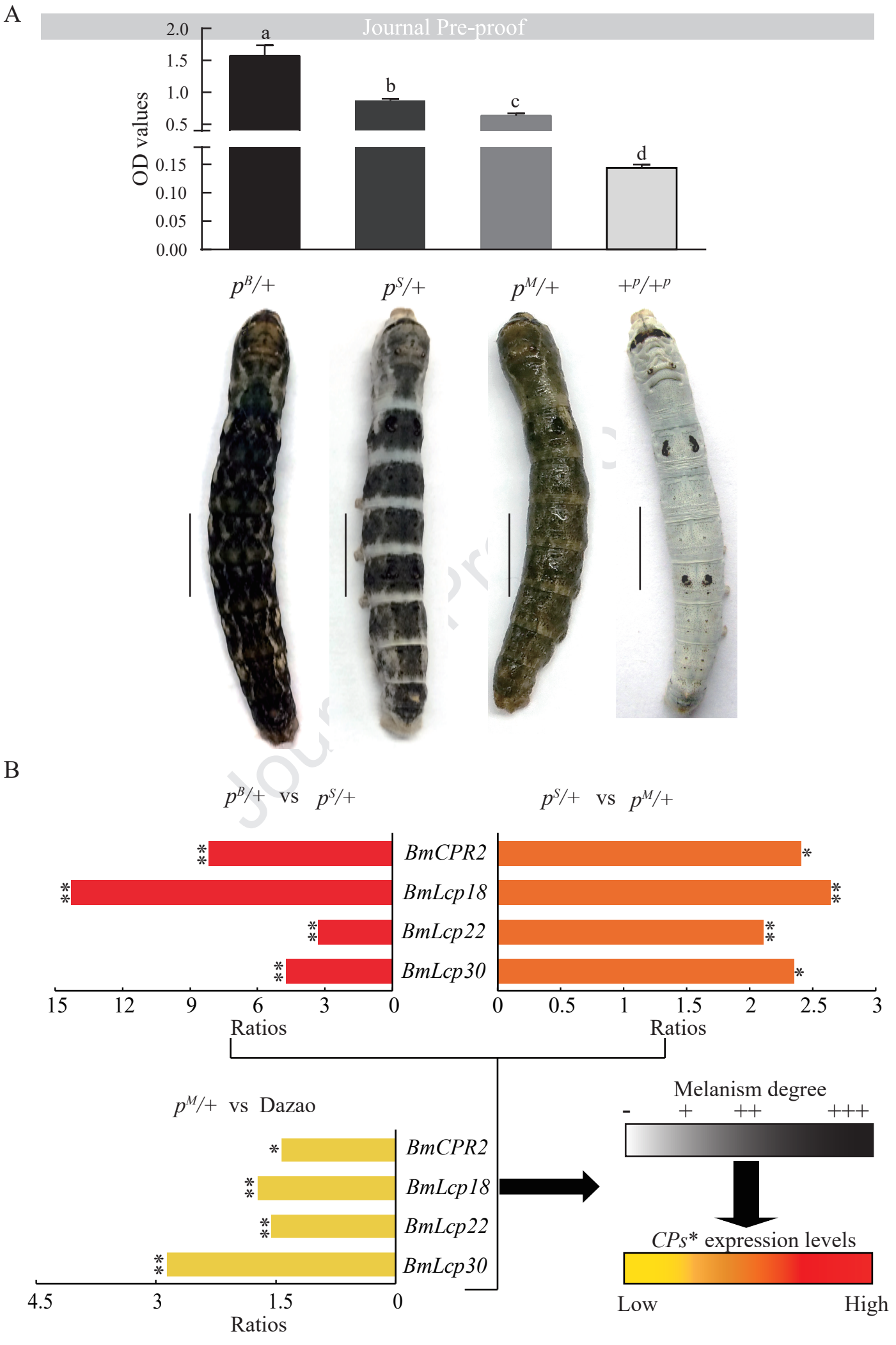
A
Journal Pre-proof
OD values
2.0
1.5
1.0
0.5
0.15
0.10
0.05
0.00
a
b
c
d
$p^B/+$
$p^S/+$
$p^M/+$
$+^p/+^p$
B
$p^B/+$ vs $p^S/+$
$p^S/+$ vs $p^M/+$
BmCPR2
BmLcp18
BmLcp22
BmLcp30
15 12 9 6 3 0
0 0.5 1 1.5 2 2.5 3
Ratios
Ratios
$p^M/+$ vs Dazao
BmCPR2
BmLcp18
BmLcp22
BmLcp30
4.5 3 1.5 0
Ratios
Melanism degree
- + ++ +++
CPs* expression levels
Low
High

Figure 4

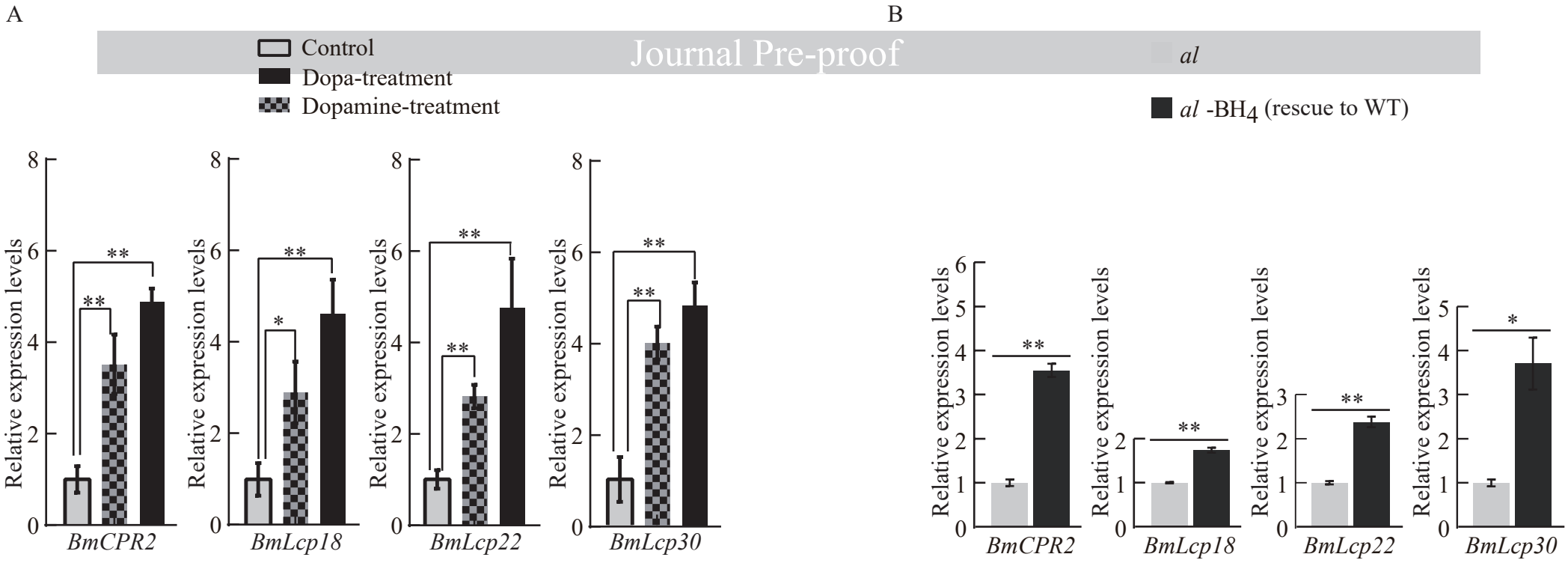

Figure 5

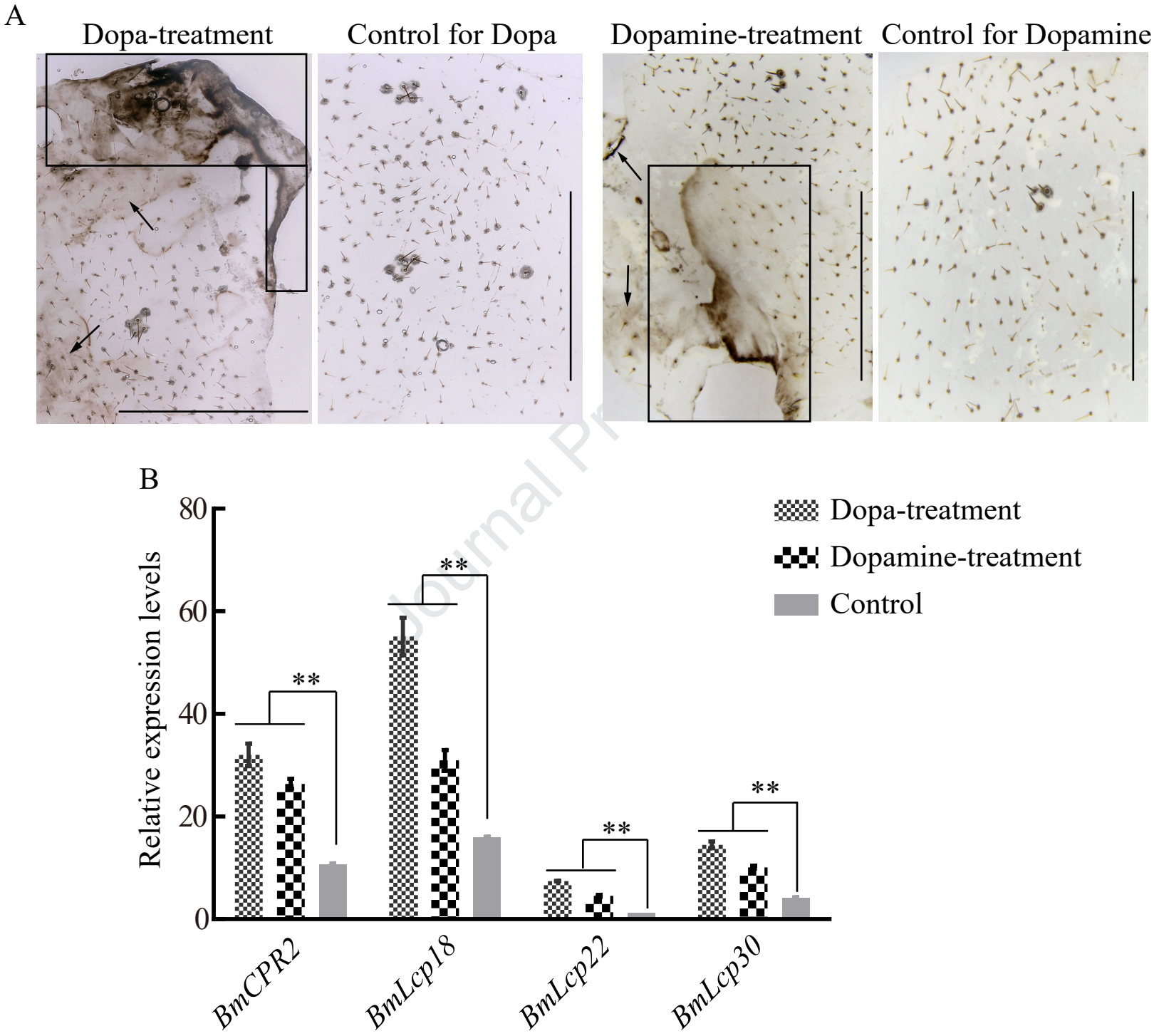
A
Dopa-treatment
Control for Dopa
Dopamine-treatment
Control for Dopamine
B
Relative expression levels
80
60
40
20
0
**
**
**
**
Dopa-treatment
Dopamine-treatment
Control
BmCPR2
BmLcp18
BmLcp22
BmLcp30

Figure 6

A

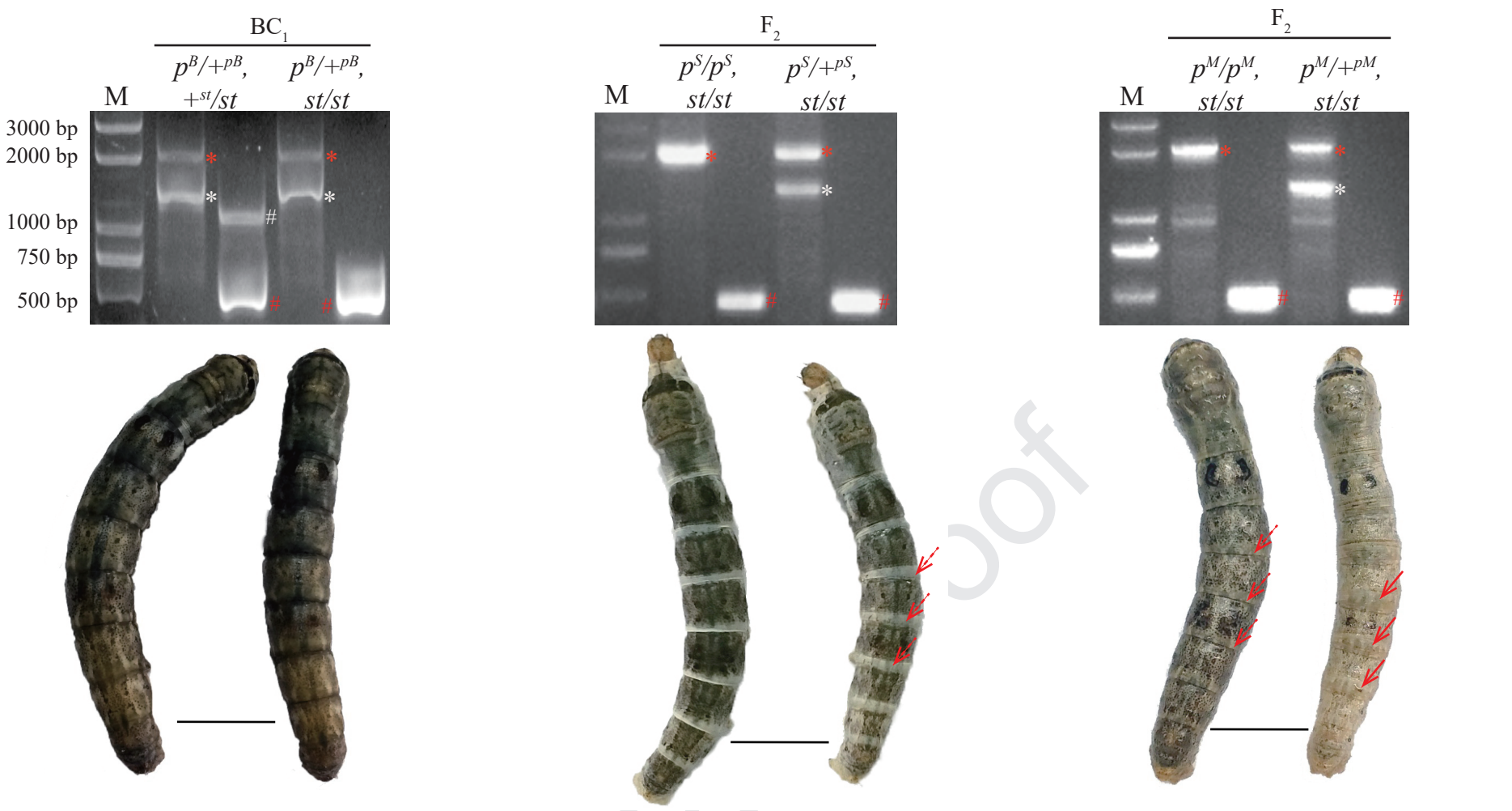

B

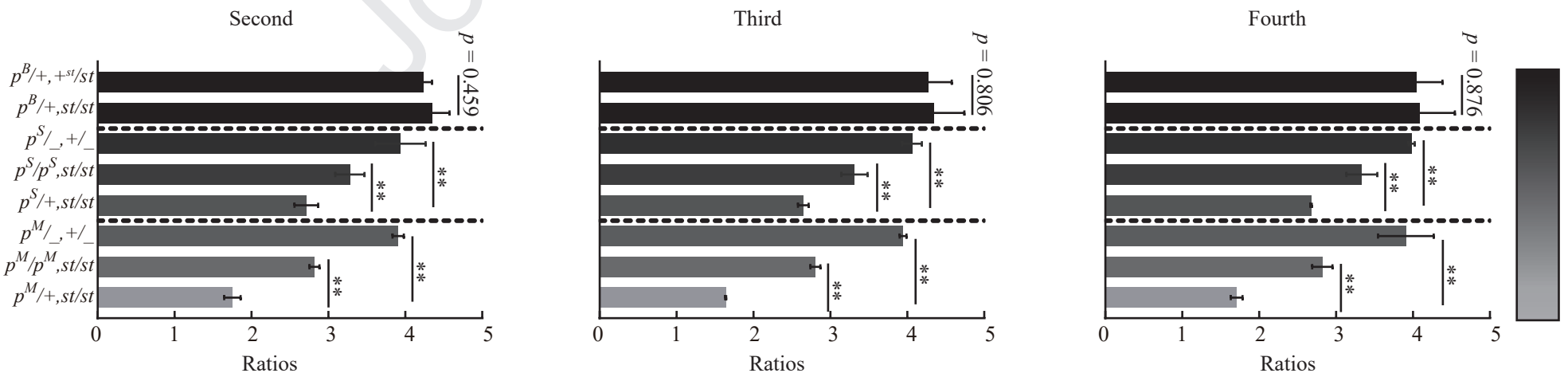

Figure 7

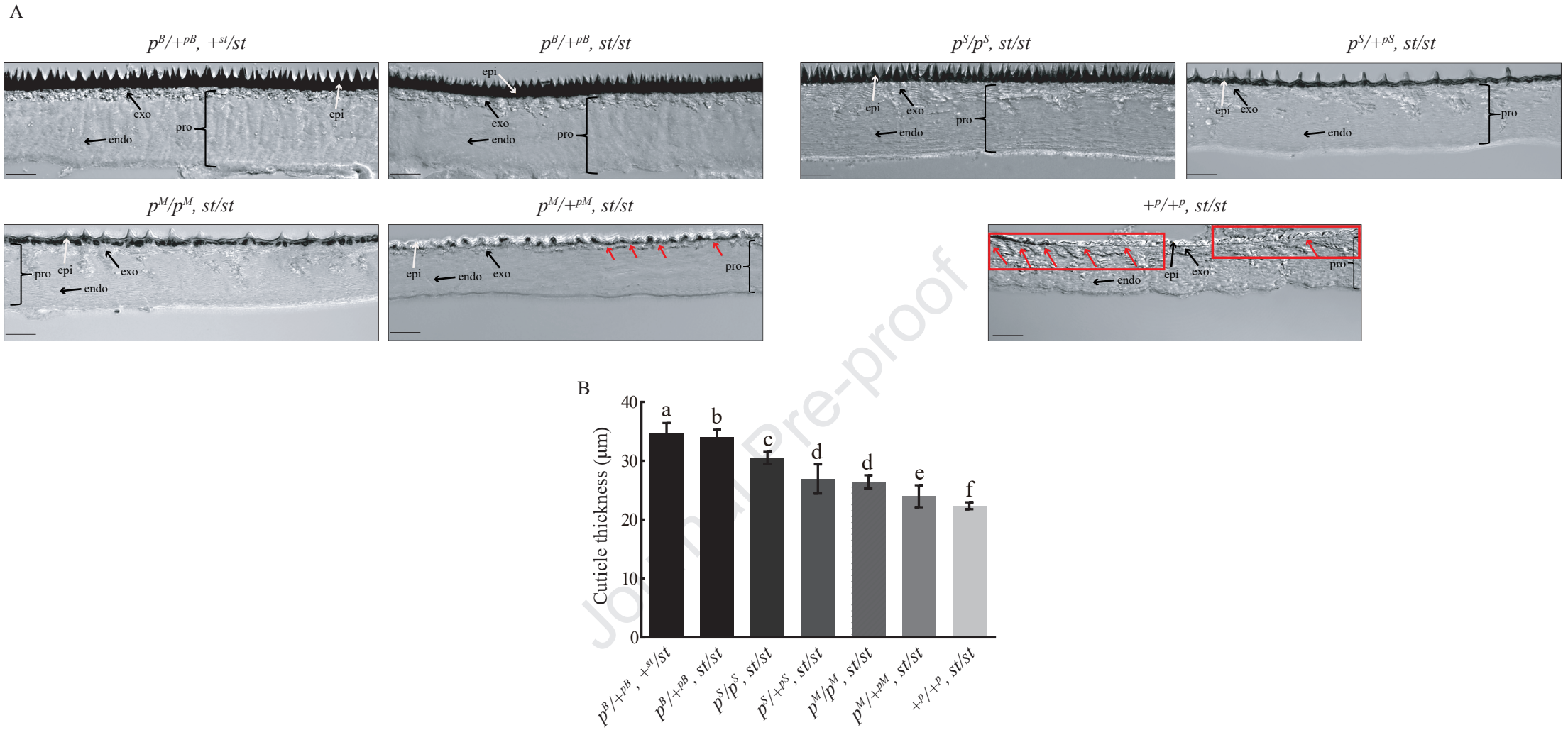

Figure 8

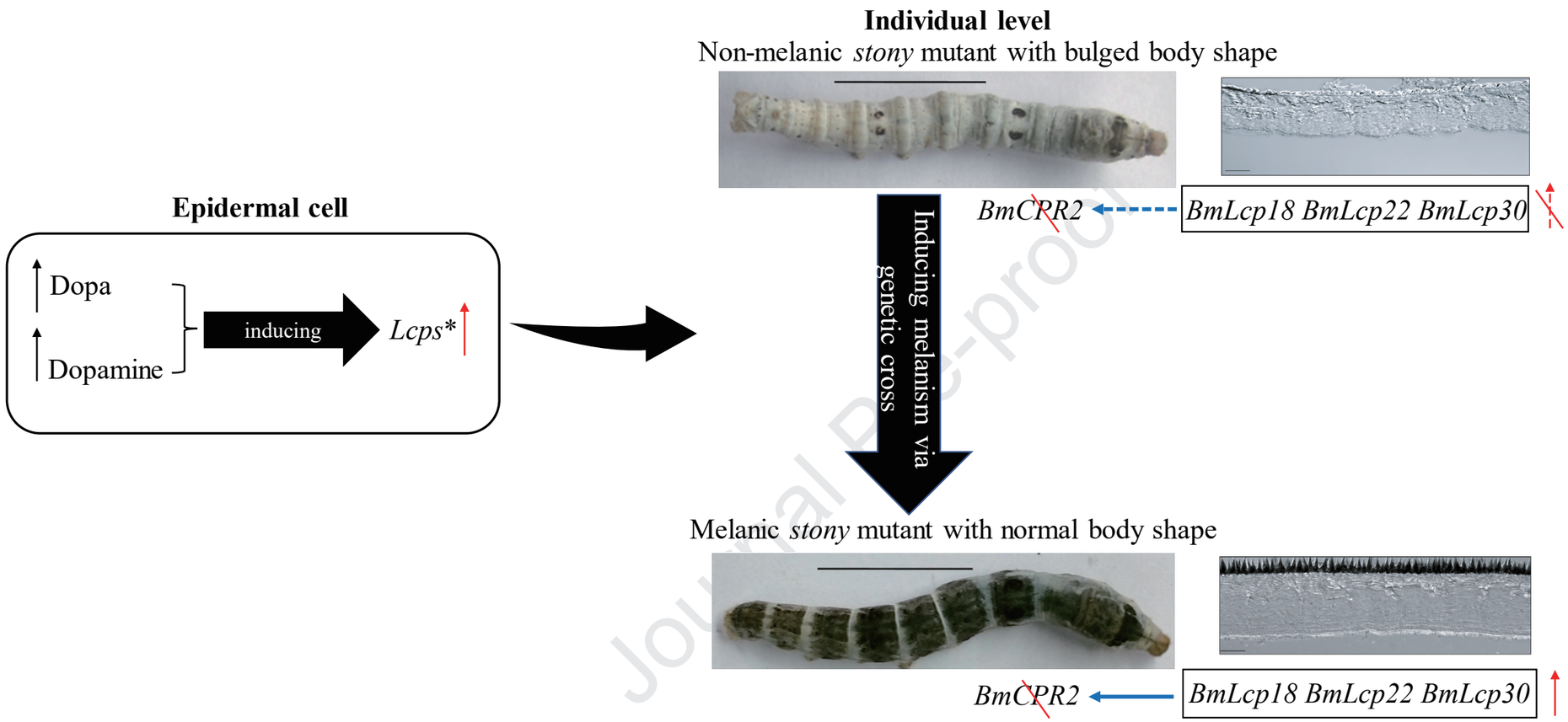
Individual level
Non-melanic stony mutant with bulged body shape
BmCPR2
BmLcp18 BmLcp22 BmLcp30
Epidermal cell
Dopa
Dopamine
inducing
Lcps*
Inducing melanism via genetic cross
Melanic stony mutant with normal body shape
BmCPR2
BmLcp18 BmLcp22 BmLcp30

Highlights

· The physical structure of melanic and non-melanic cuticle are quite different.

· The degree of melanism positively correlates with the expression of RR1-type larval cuticular protein genes.

·Melanin precursors induce the expression of RR1-type larval cuticular protein genes.

· RR1-type larval cuticular proteins with expression and chitin-binding similarity rescue cuticle defects under melanism background.

· The effect of melanin on cuticular proteins is beneficial to maintain normal larval morphological traits in *Bombyx mori*.